energy&fuels

pubs.acs.org/EF Article

Deactivation of a Biomass-Derived Zirconium-Doped Phosphorus-Containing Carbon Catalyst in the Production of Dimethyl Ether from Methanol Dehydration

Javier Torres-Liñán, Miguel García-Rollán, Juana M. Rosas, José Rodríguez-Mirasol, and Tomás Cordero*

Cite This: *Energy Fuels* 2021, 35, 17225−17240 Read Online

ACCESS | Metrics & More | Article Recommendations | Supporting Information

ABSTRACT: Dehydration of methanol to produce dimethyl ether (DME) was studied at relatively high temperatures (400−600 °C) on biomass-derived phosphorus-containing carbon impregnated with a zirconium salt. Highly thermally stable zirconium phosphate surface groups could be obtained on the final catalyst, which were responsible for the high stability and selectivity to DME of the catalyst at temperatures lower than 400 °C. However, harder operation conditions, closer to those of the industrial process, were evaluated to analyze the changes of the catalyst surface properties with the reaction temperature and the possible causes of deactivation. Thus, high methanol conversion and selectivity to DME were also observed in the temperature range of 400−600 °C, although deactivation was detected. Coke deposition was responsible for a decrease in microporosity and surface concentration of zirconium and phosphorus of the catalyst. Temperature-programmed desorption, ^{31}P magic angle spinning nuclear magnetic resonance, and X-ray photoelectron spectroscopy results suggest that the Zr−O−P groups from zirconium phosphate species were responsible for the long-term stability of the catalyst and that the C−O−P-type active sites were deactivated very fast. However, coke deposition on Zr−O−P-type active sites caused a slow and irreversible deactivation, while deposited coke on the C−O−P-type active sites was easily eliminated by the oxidative treatment in air. A reaction scheme that accounted for the gas product distribution and the production of coke was proposed. A kinetic model for coke formation as a function of time on stream that successfully represents the experimental results was also propounded, which yielded a value for the activation energy for the production of coke of 124 kJ/mol.

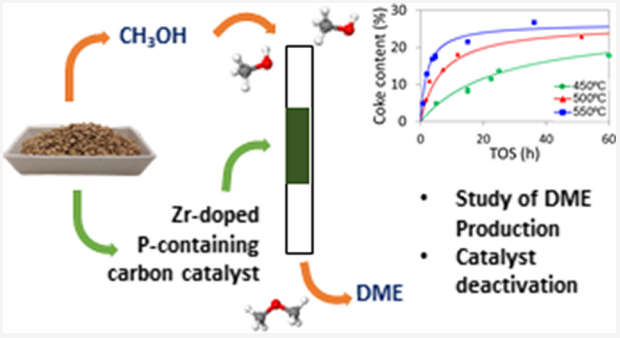

1. INTRODUCTION

Global warming, associated with an increase in CO_2 and other greenhouse gas (GHG) emissions, the significant increase in energy consumption expected in the coming decades, and the reduction of fossil fuel reserves warn of the need for a radical change in the strategy of natural resource management and in energy production and consumption.[1−4] Sustainable production of energy and chemicals plays an important role in the 2030 agenda adopted by the United Nations for achieving sustainable development and, thus, transforming the world.[5] In this sense, the implementation of new strategies for the valorization of industrial waste and lignocellulosic biomass, through the development of waste refineries[6,7] (in the transitional term) and biorefineries[8−10] (in the medium or long term), could mean interesting alternatives to finally achieve the benefits of a circular economy. That scenario requires the efficient utilization of side and waste materials from different sources (such as plastic, paper and pulp, and agroforestry industries, among others) for the sustainable generation of high-value-added biofuels, chemicals, and other bioproducts.[11]

Dimethyl ether (DME) is as a promising diesel substitute that is receiving much attention in the last decades because of its high cetane number. Moreover, its combustion generates lower emissions of hydrocarbons (HCs), NO_x, particulate matter (PM), and soot compared to diesel,[12,13] and it can be used as a liquefied petroleum gas (LPG) substitute,[14] hydrogen vector,[15,16] and propellant.[17] Several compounds of high interest in industry can also be obtained from DME, like olefins[18−20] and other HCs.[21] Thus, the industrial importance of this compound is very high, and it is expected to reach 5867.28 kiloton by 2026.[22]

Industrial production of DME is carried out from syngas in a two-stage process, where methanol is first produced on a

Special Issue: 2021 Pioneers in Energy Research: Javier Bilbao

Received: June 3, 2021
Revised: August 11, 2021
Published: August 31, 2021

https://doi.org/10.1021/acs.energyfuels.1c01721
Energy Fuels 2021, 35, 17225−17240

metallic catalyst, usually based on CuO−ZnO−Al_2O_3[23] and, in a second step, it is selectively dehydrated to DME (MTD process), using a catalyst of moderate acidity, such as γ-alumina and passivated ZSM-5.[24−27] γ-Alumina is very active and highly selective to DME. However, the hydrophilic character of this catalyst produces a collapse of its porous structure in the presence of water, which deactivates the catalyst significantly. Deposition of coke on strong acid sites of the catalyst also causes the deactivation of the catalysts.[28,29] In this sense, the use of low acidic zeolites and silicoaluminophosphates or catalyst passivation for reducing the hydrophobicity and lowering the acidity inhibits the blockage of the pore structure and the deactivation of the catalyst by coke deposition.[30,31] Nevertheless, a new way of DME production in only one step directly from syngas or even from a CO_2/H_2 mixture on a bifunctional catalyst, usually copper−zinc−alumina mixed with γ-alumina or modified zeolites, is being widely studied in recent years.[17,32] In this sense, the use of zirconium as a promoter on those bifunctional catalysts has shown an enhanced efficiency for this reaction.[33,34]

On the other hand, the fact that synthesis gas can be obtained from sustainable sources, by gasifying used plastics and tires and biomass waste,[35−38] opens up a greater possibility for DME as a cleaner alternative to produce fuels and chemicals. Professor Bilbao and his research group have been very active in studying not only the MTD process[27] but also the direct production of DME in one step[39−41] (STD process). They have provided very relevant and high-impact contributions focused on the design of novel bifunctional structured catalysts[42−44] and the development of kinetic models,[45−47] taking into account the specific reaction conditions of these processes and the catalyst deactivation. They have also studied different reactor configurations, including a packed bed membrane reactor with a highly hydrophilic membrane, for *in situ* removal of water from the reaction medium to displace the equilibrium of methanol production, its selective dehydration to DME, and the reverse water−gas shift reaction.[48,49] They have also widely analyzed the possibilities of DME as a sustainable source of hydrogen, through catalytic steam reforming,[50,51] and of light olefins, by the DME-to-olefins (DTO) process.[47,52,53] Furthermore, this research group has been very productive in studying the deactivation processes of these catalysts, both the metal and the acidic phases,[54] which are of great importance from an industrial point of view. They have proposed a relevant methodology for a simultaneous computation of the kinetic parameters of complex reaction networks and deactivation kinetics,[55] with the added difficulty of including different reactor configurations[56] and reactions involving the deposition of solid carbonaceous compounds and coke.[57]

Likewise, the efficient use of residual biomass resources in future biorefineries to sustainably produce not only fuels and chemicals but other bioproducts (such as, for instant, catalysts) also involves a relevant strategy for boosting the bio-based circular economy. In this sense, intensive research is taking place on the preparation of carbon catalysts from biomass.[58−60] With regard to the selective dehydration reaction of methanol to DME, Moreno-Castilla et al. prepared acid surface carbon catalysts by oxidation of biomass-derived activated carbons with different liquid oxidants and acids that presented some activity for this reaction related to the presence of carboxyl acid surface groups on the carbon catalysts.[61] However, the catalysts were rapidly deactivated as a result of the partial decomposition of these oxygen surface groups at the reaction temperatures.

Chemical activation of lignocellulosic materials with phosphoric acid[62,63] is a conventional method to produce activated carbons with a high porosity and relatively large surface area.[63] Activation of biomass residues with phosphoric acid under certain operation conditions (relatively high activation temperatures) generates the presence of different thermally stable phosphorus surface groups, responsible for relatively high surface acidity and oxidation resistance of the final activated carbons,[64−66] which provide these simple and low-cost carbon materials with interesting properties for applications in heterogeneous catalysis, as catalyst supports and/or catalysts themselves.[67−70] These P-containing carbon materials have shown high activity for ethanol and larger alcohol decomposition reactions, with high selectivity to dehydration products.[71−73] This type of carbon catalyst was also evaluated for the MTD process, exhibiting high initial methanol conversion and selectivity to DME. However, they showed a fast deactivation unless oxygen was present in the reaction mixture.[74]

Metal phosphate materials, like zirconium phosphate, have shown activity in alcohol dehydration reactions,[75−78] including the methanol dehydration reaction.[79] In this sense, impregnation of a porous carbon prepared by activation of a lignocellulosic waste with phosphoric acid with a zirconium salt was evaluated to make use of phosphorus present on the carbon surface, with the goal of obtaining a highly dispersed and stable zirconium phosphate active phase anchored on the activated carbon surface. The fact that the catalyst was obtained from a biomass waste by a very simple preparation method represents an advantage in terms of the sustainability of the process. In this sense, the active phase can be recovered easily at the end of the service time of the catalyst, just by gasifying the carbon support to also obtain syngas, thus boosting the bioeconomy. This catalyst showed high stability, with methanol conversions of around 50% and selectivity to DME close to 97% at 350 °C.[80,81] However, the methanol dehydration reaction takes place at very high conversion levels at industrial conditions, in which deactivation of the catalyst is mainly caused by coke deposition[82−85] produced over acid sites by solid carbonaceous precursor polymerization into high-molecular-weight species that are unable to be desorbed, covering the active site or clogging pores. The temperature has a critical importance in the quantity and type of coke formed.[86]

In the present paper, we report the evaluation of a Zr-loaded P-containing biomass-derived carbon material as a catalyst for methanol dehydration to DME under severe reaction conditions to achieve high methanol conversions, close to those that usually take place in the industrial MTD process, to analyze the activity, stability, and selectivity of this catalyst. Furthermore, the textural properties, surface chemistry, and coke content of the catalyst have been studied at different reaction temperatures and times on stream. A kinetic model to predict the coke formation at these different operating conditions has been proposed. In addition, the possible regeneration of the deactivated catalyst with an air treatment was assessed.

2. MATERIALS AND METHODS

2.1. Catalyst Preparation. Olive stone, a low-cost biomass waste material, has been used as a precursor of the carbon catalyst. Olive stone was supplied by Sociedad Cooperativa Andaluza Olivarera y

https://doi.org/10.1021/acs.energyfuels.1c01721
Energy Fuels 2021, 35, 17225−17240

Frutera San Isidro, Periana (Malaga), Spain. The precursor was initially impregnated with phosphoric acid (H_3PO_4, 85%, w/w) at a mass ratio of 2:1 (H_3PO_4/olive stone). The mixture was dried at 60 °C for 12 h and then activated in a tubular furnace, under nitrogen flow (150 Ncm^3/min, purity of 99.999%, Linde) at 800 °C for 2 h, using a heating rate of 10 °C/min. The activated sample was washed with distilled water at 60 °C until a constant pH in the residual water. After drying, the chemically activated carbon (ACP) was impregnated by the incipient wetness method with zirconium(IV) oxynitrate hydrate ($N_2O_7Zr{\cdot}xH_2O$, purity of 99%, Sigma-Aldrich). The sample was loaded with 5.25% zirconium, which turned out to be the optimum amount of deposited zirconium for methanol to DME reaction at lower temperatures in a previous work.[80] The impregnated samples were then dried for 12 h at 120 °C and treated at 250 °C for 2 h under an air atmosphere. A detailed description of the catalyst preparation can be found elsewhere.[80]

2.2. Characterization. Textural characterization of the catalyst (before and after reaction) was conducted by N_2 adsorption−desorption at −196 °C and CO_2 adsorption at 0 °C in an ASAP 2020 instrument (Micromeritics). Every sample was outgassed at least for 8 h at 150 °C before the analysis. From the N_2 isotherm data, the apparent surface area (A_{BET}) was obtained using the Brunauer−Emmett−Teller (BET) equation,[87] the micropore volume (V_t) and external surface area (A_t) were calculated by the t-plot method,[88] and the mesopore volume (V_{mes}) was obtained as the difference between the maximum volume adsorbed (V_{tot}) at a relative pressure of 0.995 and the micropore volume. From the CO_2 isotherm, the narrow micropore volume (V_{DR}) and narrow surface area (A_{DR}) were calculated applying the Dubinin−Radushkevich equation.[89] Pore size distributions were obtained from N_2 isotherm data using two-dimensional non-local density functional theory (2D-NLDFT) heterogeneous adsorption models for carbon slit-shaped pores.[90]

Surface chemistry of fresh and spent catalysts were analyzed by X-ray photoelectron spectroscopy (XPS), temperature-programmed desorption (TPD), and ^{31}P magic angle spinning (MAS) nuclear magnetic resonance (NMR). XPS analyses were also carried out in a spectrophotometer 5700C (Physical Electronics) with Mg Kα radiation (1253.6 eV). The C_{1s} peak is located at 284.5 eV and used as a reference to place the rest of the peaks. TPD is usually used to characterize the oxygen functional groups presented in the bio-based carbon surface, which are formed during carbonization/activation processes. Typically, for the TPD analyses, 150 mg of sample was introduced in a crucible and heated in N_2 flow (200 Ncm^3/min, purity of 99.999%, Linde) from room temperature to 1500 °C at a heating rate of 10 °C/min. CO and CO_2 evolved amounts at different temperatures were determined by a non-dispersive infrared (NDIR) gas analyzer (Siemens ULTRAMAT 22) and were related to the surface oxygen-containing functional groups. ^{31}P MAS NMR spectroscopy was carried out at room temperature using a high-resolution Bruker AXS spectrometer, model AVANCEIII HD 600 (narrow bore). The magnetic field was 14.1 T corresponding to a ^{31}P resonance frequency of 242.92 MHz. The spinning rate was 15 kHz. $NH_4H_2PO_4$ was used as a reference at 0 ppm. $^{31}P-^{1}H$ heteronuclear correlation (HETCOR) NMR spectra were also recorded using a triple resonance cross-polarization (CP)-MAS probe of 3.2 mm. ^{31}P MAS NMR spectra were recorded with a 2 ms contact pulse and 1 s delay with ^{1}H decoupling (^{31}P high-power decoupling (HPDEC) with spinal decoupling sequence of 64 for P) and summing up 200 scans.

2.3. Catalytic Dehydration of Methanol. Catalytic performance of the zirconium-impregnated P-containing activated carbons was evaluated for the dehydration of methanol to DME reaction. The experiments were carried out in a fixed-bed microreactor (4 mm inner diameter) located in a vertical furnace, working under atmospheric pressure, with a catalyst mass of 150 mg. Methanol (CH_3OH, purity of 99.9%, Carlo Erba) was fed to the reactor using a syringe pump (Cole-Parmer 74900-00-05 model), and the inlet stream was maintained at a methanol partial pressure of 0.04 atm in a 70 Ncm^3/min helium flow (purity of 99.999%, Linde). The reaction temperature ranged from 450 to 600 °C, and a space time of 75 g_{cat} s $mmol_{CH_3OH}^{-1}$ was used. All of the pipelines were heated at 120 °C to avoid methanol or any other product condensation.

Concentrations of gas reactants and products were measured by an online Varian CP-4900 gas microchromatograph (Agilent), equipped with capillary columns: 5A molecular sieve, PPQ, and wax columns.

Conversion and selectivity were defined by the following expressions:

$$X = \frac{F_{CH_3OH_0} - F_{CH_3OH}}{F_{CH_3OH_0}} \quad (1)$$

$$S = \frac{n_i F_i}{\sum n_i F_i} \quad (2)$$

where X represents the conversion, S denotes the selectivity, $F_{CH_3OH_0}$ is the methanol molar flow fed to the reactor, F_{CH_3OH} is the methanol molar flow in the outlet stream, F_i stands for the molar flow of the product i in the outlet stream, and n_i represents the number of carbon atoms in the corresponding i molecule. The coke content was quantified by direct weighing of the catalyst before and after reaction, and coke selectivity was calculated by assuming that the produced coke consisted of pure carbon.

Air treatment of the deactivated catalysts after reaction was carried out *in situ* by an air flow (purity of 99.999%, Linde) of 70 cm^3/min. Samples, after reaction at different experimental conditions, were exposed to air at 200 °C followed by a temperature increase to 350 °C at a heating rate of 10 °C/min. This temperature was kept for 2 h.

3. RESULTS AND DISCUSSION

3.1. Catalyst Characterization. Figure 1 represents the N_2 adsorption−desorption isotherm at −196 °C of the fresh catalyst. The catalyst shows a type IV(a) isotherm with a large nitrogen adsorption volume at low relative pressures, evidencing the presence of high micropore volumes. In addition, a H4 hysteresis loop is also observed at a medium−high range of relative pressures, associated with the adsorption in mesopores of an in-bottle shape.[91] Table 1 collects the textural parameters derived from the N_2 and CO_2 adsorption isotherms. CO_2 adsorption at a low relative pressure (<0.3) and 0 °C was used to characterize narrow microporosity (pores lower than 0.7 nm) as a result of a better diffusion in these narrow micropores compared to that of the N_2 adsorption at −196 °C. Nevertheless, the catalyst showed a micropore volume value measured by adsorption of N_2 (V_t)

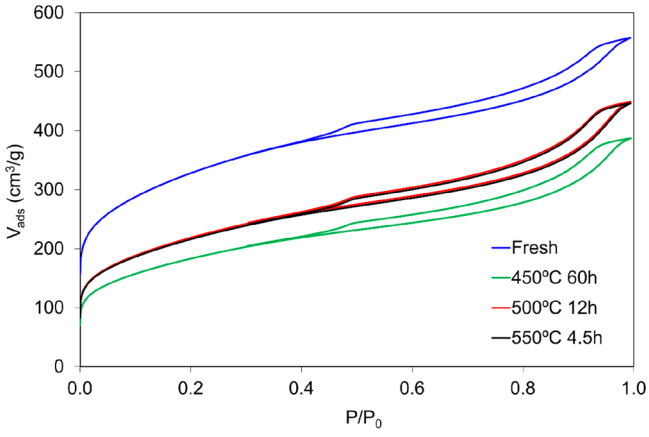

Figure 1. N_2 adsorption−desorption isotherms at −196 °C of fresh and spent catalysts with the same coke content (18%) obtained at different reaction temperatures and TOS at a methanol partial pressure of 0.04 atm and a space time of 75 g_{cat} s $mmol_{CH_3OH}^{-1}$.

https://doi.org/10.1021/acs.energyfuels.1c01721
Energy Fuels 2021, 35, 17225−17240

Table 1. Textural Parameter Values Derived from the N_2 Adsorption Isotherm at −196 °C and CO_2 Adsorption Isotherm at 0 °C of Fresh and Spent Catalysts with Different Coke Contents Obtained at Different Reaction Temperatures and TOS at a Methanol Partial Pressure of 0.04 atm and a Space Time of 75 g_{cat} s $mmol_{CH_3OH}^{-1}$

		N_2 isotherm					CO_2 isotherm	
sample	coke content (%)	A_{BET} (m^2/g)	A_t (m^2/g)	V_t (cm^3/g)	V_{mes} (cm^3/g)	V_{tot} (cm^3/g)	A_{DR} (m^2/g)	V_{DR} (cm^3/g)
fresh		1130	271	0.44	0.42	0.86	476	0.19
450 °C for 60 h	18	644	215	0.22	0.38	0.60	238	0.10
500 °C for 12 h	18	767	248	0.27	0.43	0.69	281	0.11
550 °C for 4.5 h	18	757	246	0.26	0.43	0.69	273	0.11
500 °C for 3 h	11	909	282	0.32	0.47	0.79	314	0.13
500 °C for 7 h	14	806	257	0.28	0.44	0.72	286	0.11
500 °C for 51 h	23	600	154	0.23	0.26	0.48	236	0.09

significantly higher than the value determined by CO_2 adsorption (V_{DR}), which also suggests the presence of broad microporosity. In addition, the relatively high values of the external surface area (A_t) and mesopore volume (V_{mes}) are also indicative of the large contribution of mesoporosity found in this sample. Table S1 of the Supporting Information summarizes the atomic surface concentrations of the catalyst derived from XPS analysis. The results showed the presence of mainly carbon and oxygen species and, to a less extent, phosphorus and zirconium surface groups. In this sense, the P/Zr ratio was close to 1, lower than the theoretical zirconium phosphate atomic ratio (it should be 2), which could be attributed to an excess of zirconium deposited during wet impregnation. This result suggests the further formation of other Zr surface groups, such as Zr−C/Zr−$(O-C)_2$ groups, which were also observed in a previous work,[81] close to those of zirconium phosphate species, as well as phosphorus−carbon surface groups.

3.2. Catalyst Performance. Methanol conversions as a function of time on stream (TOS) at temperatures between 300 and 600 °C are represented in Figure 2 for a methanol

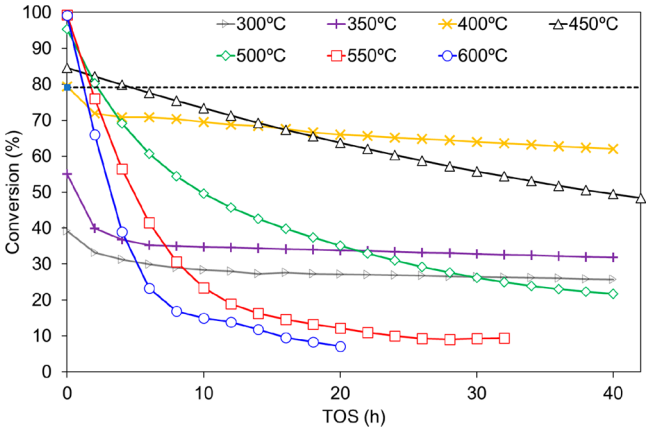

Figure 2. Methanol conversion profile as a function of TOS at different reaction temperatures at a methanol partial pressure of 0.04 atm and a space time of 75 g_{cat} s $mmol_{CH_3OH}^{-1}$. The dashed line shows the equilibrium methanol−DME conversion at 450 °C.

partial pressure of 0.04 atm and a space time of 75 g_{cat} s $mmol_{CH_3OH}^{-1}$. Steady-state conversions of methanol were observed for temperatures lower than 450 °C, with a conversion value higher than 60% for a reaction temperature of 400 °C, which indicates that the catalyst presents a high stability for methanol dehydration in this temperature range. An increase in the reaction temperature produced a significant enhancement of the initial methanol conversion (short TOS), with conversion values of 100% for temperatures higher than 500 °C. However, a slight reduction of methanol conversion with TOS was observed for a reaction temperature of 450 °C, and this decay was somewhat more pronounced as the temperature increased. In this sense, the methanol conversion value remained higher than 50% at 450 °C for more than 24 h under the studied conditions. However, this value was lower than 5% at a reaction temperature of 600 °C for similar TOS (24 h).

In this regard, the use of carbons with acid surface groups as catalysts to produce DME from dehydration of methanol was evaluated, but reaction temperatures could not exceed 180 °C because the catalysts suffered from a strong catalyst deactivation by decomposition of the acid surface groups, showing a maximum conversion of around 13% at this temperature.[61] On the other hand, the $H_3PW_{12}O_{40}$ heteropolyacid catalyst also showed faster deactivation during methanol dehydration at milder conditions, with conversion decreasing from 33 to 14% after 2 h at 200 °C for a catalyst weight/volume flow rate (W/F_{CH_3OH}) = 7.33 g_{cat} s $mmol_{CH_3OH}^{-1}$ (although some deactivation was already detected at 150 °C).[85]

In the present study, the methanol conversion values for temperatures higher than 400 °C at short TOS exceed those of the methanol−DME reaction equilibrium at the corresponding temperature (represented as dashed lines in Figure 2), which suggests that side reactions were carried out, like those involved in coke production.

Figure 3 shows the gas outlet concentrations as well as the selectivity as a function of TOS at different reaction temperatures, also including the selectivity to coke. DME and water were the only products observed at a reaction temperature of 400 °C (Figure 3a), with trace methane at very short TOS and, therefore, with a very high selectivity to DME (99%) with TOS (Figure 3b). Figure 3c shows the gas outlet concentrations as a function of TOS for the catalyst at 450 °C. A decay of the DME concentration with TOS was observed, as a consequence of a gradual reduction in the methanol conversion as well (shown in Figure 2). However, the selectivity to DME (Figure 3d) remained stable at this temperature, with values higher than 90% for more than 20 h. A small amount of methane and coke and, to a less extent, CO could also be detected. At 550 °C (panels e and f of Figure 3), DME and water outlet concentrations decreased faster and methane and coke formation becomes more important than at 450 °C, although DME selectivity was still quite high, showing

https://doi.org/10.1021/acs.energyfuels.1c01721
Energy Fuels 2021, 35, 17225−17240

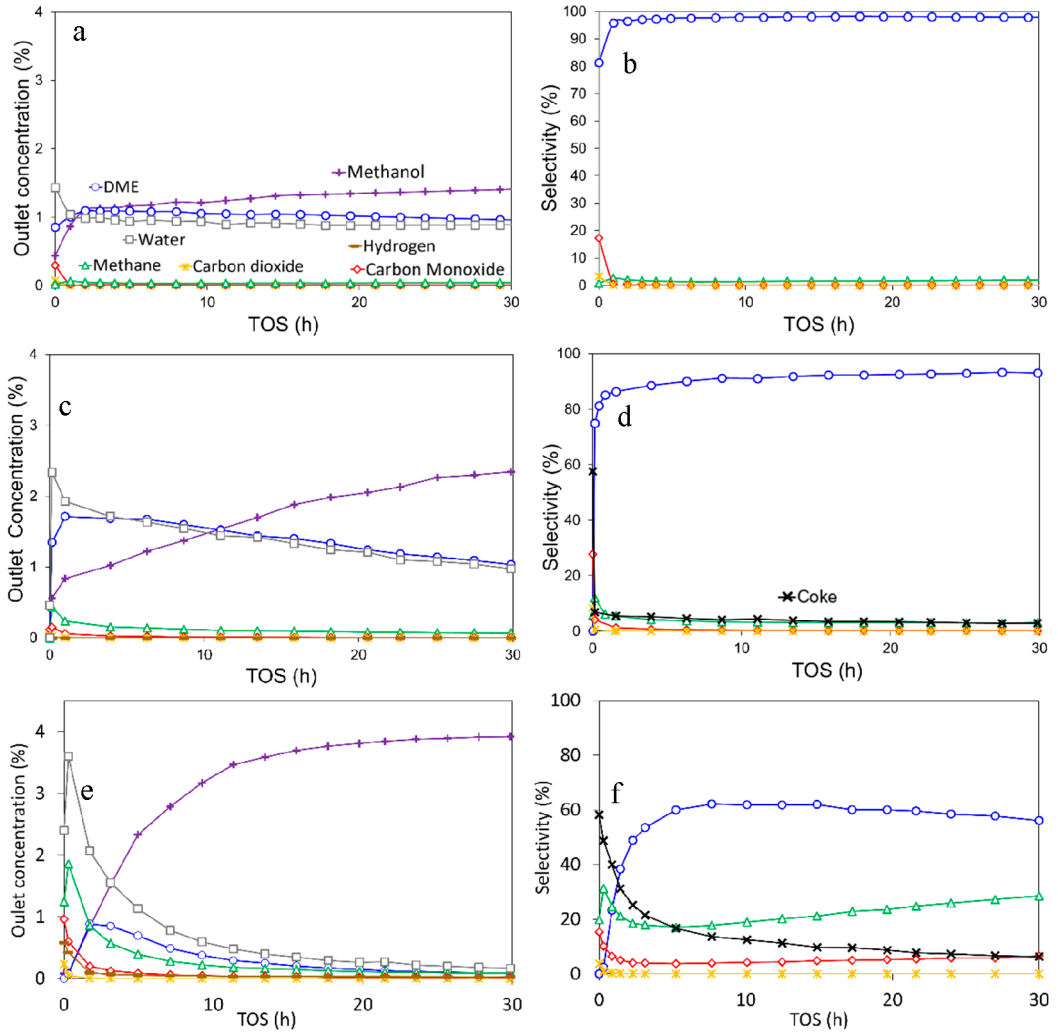

Figure 3. (a, c, and e) Gas outlet concentrations and (b, d, and f) selectivity to carbon products as a function of TOS at (a and b) 400 °C, (c and d) 450 °C, and (e and f) 550 °C, respectively, at a methanol partial pressure of 0.04 atm and space time of 75 g_{cat} s $mmol_{CH_3OH}^{-1}$: methanol (purple pluses), DME (blue circles), methane (green triangles), carbon monoxide (red diamonds), carbon dioxide (yellow asterisks), hydrogen (brown rectangles), water (gray squares), and coke (black crosses).

values higher than 55% for more than 35 h. Thus, the relatively high selectivity to DME observed for the catalyst studied in the present work should be highlighted, especially considering that several works found in the literature, which studied different acid catalysts for dehydration of methanol, showed lower selectivity to DME values even at lower temperatures (<350 °C), although other operation conditions were also different (space time). For example, γ-alumina showed a selectivity to DME of 85% at 400 °C;[24] selectivity to DME in several kinds of HZSM-5 decayed almost totally as the temperature increased up to 320 °C;[92] selectivity to DME was also reduced to 80% at 400 °C for a K-modified H-ZSM5;[26] and selectivity of $H_3PW_{12}O_{40}$ decreased to 70% after 2 h at 250 °C.[85]

On the other hand, it was observed that the higher the temperature, the higher the amount of methane formed. In this sense, Akarmazyan et al.[24] associated CO and CH_4 production to a change in the mechanism as a result of the increase in the temperature. They reported that CO and CH_4 were produced as a result of the evolution of surface formate groups, which were formed instead of methoxy groups at high temperatures. To evaluate the possible thermal decomposition of DME under the conditions studied, an experiment with 3 vol % DME up to 600 °C in the absence of catalyst was carried out. The results indicated that the homogeneous DME thermal decomposition was lower than 1%, producing mainly CH_4 and CO. Therefore, the formation of methane via thermal decomposition of DME was neglected. On the other hand, Akarmazyan et al.[24] proposed that DME-adsorbed species could decompose to CH_4, H_2, and CO, but this would require the stoichiometric formation of methane and CO. Other authors also suggested the thermal decomposition of DME into CO and CH_4 or formaldehyde (that decomposes into CO + H_2).[93] The larger observed formation of methane and water than CO and DME, respectively, at 550 °C suggests that other reactions might be taking place, like the formation of methane and formaldehyde by decomposition of DME-adsorbed species (produced by the reaction of methoxy species with methanol through a six-member-ring electron transfer process), as suggested by Cheng et al.[79] Formaldehyde would decompose further to CO and H_2 or to coke (C) and H_2O, probably on different acid sites. The results observed in panels e and f of Figure 3 suggest that the second route (producing coke and water) seems to be the route that occurs to a greater extent. In

https://doi.org/10.1021/acs.energyfuels.1c01721
Energy Fuels 2021, 35, 17225−17240

this sense, the concentration of produced water and DME were very similar at 450 °C, except for initial TOS (probably as a result of water being desorbed easier than DME), evidencing that mostly all of the water comes from the methanol dehydration reaction. Nevertheless, the concentration of water greatly exceeded that of DME at 550 °C, which could be initially associated with the production of light olefins. However, olefins were hardly detected in the gas product at any of the temperatures studied. Thus, the similarities found for the production of water and coke with TOS at 550 °C (panels e and f of Figure 3) indicate that coke production and growth, through reaction of coke with oxygenated compounds (methanol and/or DME), seem to be mainly responsible for the excess observed in the water production.[94]

3.3. Characterization of the Deactivated Catalyst. The catalyst was characterized after reaction at different temperatures and TOS. N_2 adsorption−desorption isotherms at −196 °C of the spent catalyst after reaction at different experimental conditions but with the same coke content (18%) are also shown in Figure 1. Lower adsorption uptakes at low relative pressures were observed for the spent catalyst samples compared to that for the fresh catalyst, with the adsorption isotherm profile remaining similar, which suggests that coke deposition took place preferentially in micropores at all of the evaluated temperatures. A slightly larger reduction in the nitrogen-adsorbed volume at low relative pressures was observed for the catalyst deactivated at 450 °C. The three samples contained the same coke content, but the coke formation rate is obviously slower at 450 °C, needing more than 60 h to reach this amount (18%) of coke. This lower coke formation rate could favor the diffusion of methanol inside the narrow micropores, producing a higher decrease of the microporosity. The results show that microporosity was reduced by half (V_t from 0.44 to 0.22 cm^3/g) but mesoporosity remained practically the same (V_{mes} from 0.42 to 0.38 cm^3/g). Nevertheless, the remaining surface area on the spent catalysts was high enough to question that the pore filling by coke was the only cause for catalyst deactivation at these temperatures; therefore, the coverage of the active site should also play an important role in this process.

The pore size distribution of these samples is collected in Figure S1 of the Supporting Information. The catalyst presents a bimodal distribution, showing two main peaks with two maxima located at 0.63 and 2.1 nm, respectively. The spent catalysts obtained after reaction at the different experimental conditions studied showed a similar pore size distribution, but the decrease observed for the shoulder located at lower pore sizes was larger than the peak corresponding to higher pore sizes, suggesting that coke is preferentially deposited in narrow micropores rather than in wider micro- or mesopores.

Porosity of the catalyst after reacting at 500 °C for different TOS was also studied. Figure 4 collects their corresponding N_2 adsorption−desorption isotherms obtained at −196 °C. This temperature (500 °C) was chosen as the best option between high coke deposition and enough time difference between selected TOS. The percentage of deposited coke was added to the legend of Figure 4. The isotherm profile remained the same, but there was a significant reduction in the adsorbed volume at low relative pressures with the increase of the amount of coke deposited on the catalyst, associated with the preferential deposition of the carbonaceous solid on the narrow micropore surface. Table 1 lists the textural parameters of the spent catalyst after reaction at 500 °C for different TOS.

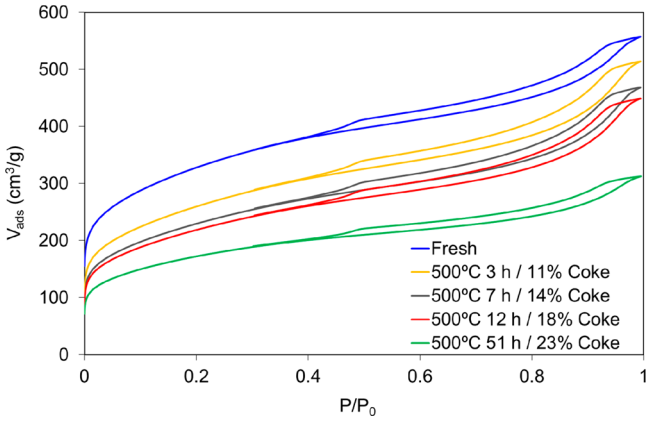

Figure 4. N_2 adsorption−desorption isotherms at −196 °C of fresh and spent catalysts with different coke contents obtained at 500 °C and different TOS at a methanol partial pressure of 0.04 atm and a space time of 75 g_{cat} s $mmol_{CH_3OH}^{-1}$.

A reduction in the BET surface area and micropore volume measured with N_2 was mainly observed at low TOS; meanwhile, the mesopore volume slightly increased. With the increase of TOS, the deposition of coke augmented too, taking place on both micro- and mesopore surfaces, as evidenced the reduction observed of about 50% for all of the textural parameter values. These results suggest that, initially, coke was deposited mainly on the surface of the micropores, and during the course of the reaction, the deposition took place uniformly on all of the catalyst surface, reaching an apparent surface area of 600 m^2/g and mesopore volume of 0.26 cm^3/g after ∼50 h of reaction at 500 °C. The pore size distribution of the spent catalyst at different TOS (Figure S2 of the Supporting Information) also confirmed the preferential deposition of coke in narrow micropores (with a mean pore size of 0.63 nm), in the same way that it happened at different reaction temperatures (see Figure S1 of the Supporting Information).

XPS analyses were performed to assess how coke deposition took place on the catalyst surface. Table S1 of the Supporting Information collects the atomic surface concentration of the catalyst after reaction at 500 °C and different TOS. As expected, the carbon surface concentration increased with TOS. This increase was accompanied by a reduction in the oxygen surface concentration, which seems to indicate that the composition of coke deposited was made up preferentially of less oxygenated species. Phosphorus and zirconium concentrations also decrease with TOS. In this sense, the fresh catalyst showed a P/Zr ratio next to 1, but this ratio increases after reaction. Specifically, the P/Zr ratio comes closer to 2, which is in concordance with the presence of zirconium phosphate species on the surface of the deactivated catalyst. On the other hand, the rapid increase observed for the P/Zr and C/Zr ratios compared to that of C/P for short TOS (3 h) indicates that the loss of the surface concentration of zirconium is much higher than that of phosphorus at the first stages.

Figure 5 shows XPS spectra of P_{2p} and Zr_{3d} of fresh and spent catalysts. The P_{2p} spectrum (Figure 5a) of the fresh sample showed a broad band that suggests the presence of different phosphorus species. The peak located at 133.2 ± 0.2 eV was attributed to $C-PO_3/C_2PO_2$ surface groups; another peak appearing at 134.0 ± 0.2 eV was attributed to $C-O-PO_3$ surface groups;[72] and a last contribution at 134.6 ± 0.2 eV was associated with zirconium phosphate surface groups, like in

https://doi.org/10.1021/acs.energyfuels.1c01721
Energy Fuels 2021, 35, 17225−17240

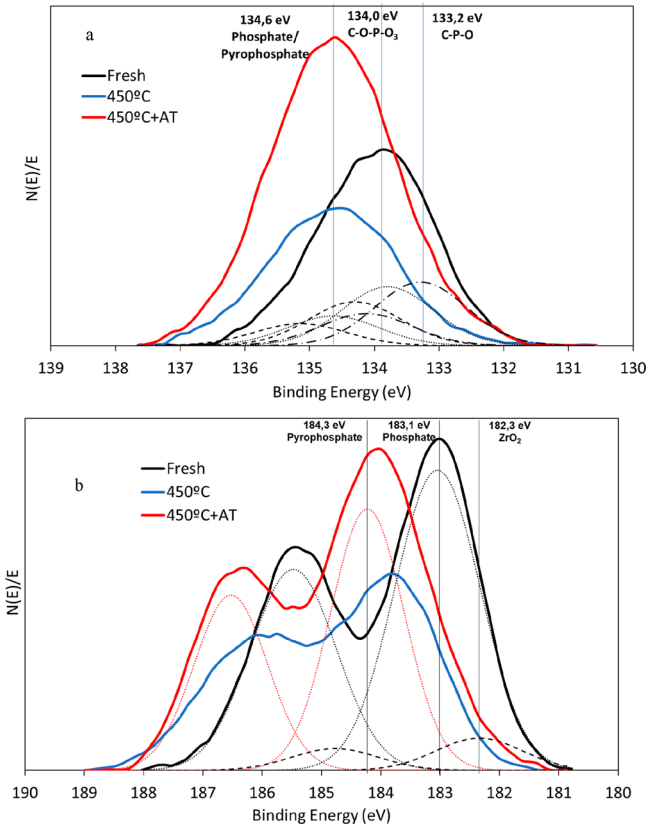

Figure 5. XPS spectra of (a) P_{2p} and (b) Zr_{3d} of fresh and spent catalysts with different coke contents obtained at 450 °C for 15 h at a methanol partial pressure of 0.04 atm and a space time of 75 g_{cat} s $mmol_{CH_3OH}^{-1}$ and after an air treatment at 350 °C.

$Zr(HPO_4)_2{\cdot}H_2O$.[95] For the sample obtained after reaction at 450 °C, a general decrease of the intensity of the whole band was observed but especially the contribution at lower binding energies, related to the coverage of C−PO_3/C_2PO_2 and C−O−P groups by coke. These results are in concordance with those reported by Valero-Romero et al.[74] with a catalyst similar to that studied in the present work. They suggested the presence of different P surface groups (such as P−OH and C−O−P) with different acid strengths, which are very quickly deactivated by coke under the methanol dehydration reaction, even at lower temperatures.

With focus on the Zr_{3d} spectrum of the fresh catalyst (Figure 5b), different Zr species could be suggested, given the presence of one peak located at 182.3 ± 0.2 eV attributed to the existence of zirconium−carbon/ZrO_2 species,[96] another peak located at 183.0 ± 0.2 eV associated with Zr−OH bonds, like in $Zr(HPO_4)_2{\cdot}H_2O$,[95] which seems to be the most relevant, and the last peak located at 184.2 ± 0.2 eV attributed to the presence of Zr(IV) bound to an electroactive species, such as phosphorus in the form of pyrophosphate groups.[97] The intensity of the spectrum decreased and shifted at higher binding energies for the sample obtained after reaction at 450 °C. These results suggest that deposition of coke took place on zirconium-phosphate-like active sites and zirconium−carbon/ZrO_2 species. Actually, the band with the peaks associated with these two species almost disappeared after reaction at 450 °C, shifting to higher binding energies, which suggests the formation of zirconium-pyrophosphate-like species, probably as a result of the attack of oxygenated compounds to the −OH group of zirconium phosphate forming methoxy and other organic groups,[98] which would be the precursors of the formed coke.

3.4. Oxidative Air Treatment over Deactivated Catalysts. Using the catalyst at different temperatures and TOS, catalysts with different degrees of deactivation by coke deposition were obtained. These deactivated catalysts were treated under an air atmosphere with the goal of oxidizing the coke deposits and regenerating the catalyst. Thus, the catalysts deactivated at 450 °C (partially) and 550 °C (almost totally) for 15 h (containing 9 and 22% of deposited coke, respectively) were treated with an air flow of 150 cm^3/min at 350 °C for 2 h (time enough to consume the deposited coke that could be oxidized under these operating conditions). Then, the oxidized catalysts were evaluated again under the same reaction conditions. A blank experiment was also performed (not shown) in which the fresh catalyst was exposed to the same air treatment prior to the dehydration reaction of methanol to DME at 450 °C. No changes in conversion or selectivity were observed in comparison to the those of the fresh catalyst without any treatment. In addition, the analysis of the mass loss during the air treatment of the catalyst obtained after reaction at 450 °C for 15 h showed a very low catalyst loss, around 4.0%. This value was practically the same as that observed for the fresh catalyst after the same oxidation treatment (blank experiment), suggesting that gasification of the formed coke was very low at this temperature.

The methanol conversions for the fresh catalyst at 450 and 550 °C and those of the corresponding deactivated samples followed by the oxidative air treatment are represented in Figure 6. The methanol conversions for the air-treated deactivated catalyst at 450 °C (second part of Figure 6a) were almost restored (in comparison to that of the fresh catalyst; first part of Figure 6a) but only initially, decreasing very fast and reaching conversion values similar to those observed for the fresh catalyst after 15 h of reaction at very short TOS. In the case of the reaction temperature of 550 °C, the conversion of methanol for the oxidized deactivated (almost totally) catalyst could not be totally restored, taking only 3 h to reach the same residual conversion as that observed for the fresh catalyst after 15 h of reaction.

The catalyst support (not containing Zr but containing P surface groups) oxidized in air flow at the same conditions was also analyzed at these reaction temperatures to be compared to the fresh and deactivated catalysts followed by this oxidative treatment (results included in panels a and b of Figure 6). In this sense, Rosas et al. reported the preferential oxidation of C−P−O groups to C−O−PO groups (to that of other surface groups) on phosphorus-containing activated carbon surfaces under an air atmosphere and similar temperature conditions.[65] This C−O−PO surface group also presented moderate-strength acidity, as reported by Valero-Romero et al.[74] On the other hand, Palomo et al.[80,81] suggested that Zr−O−P sites, present in zirconium phosphate surface species of carbon-based catalysts, were responsible for the activity of these catalysts for the dehydration of methanol to DME.

Figure 6b show that the oxidized catalyst support showed a very fast deactivation for methanol dehydration at both reaction temperatures, showing a conversion profile (in both cases) similar to that observed for the oxidized deactivated catalyst reacting at 550 °C. These results suggest the presence of, at least, two types of coke, probably of different nature, on

https://doi.org/10.1021/acs.energyfuels.1c01721
Energy Fuels 2021, 35, 17225−17240

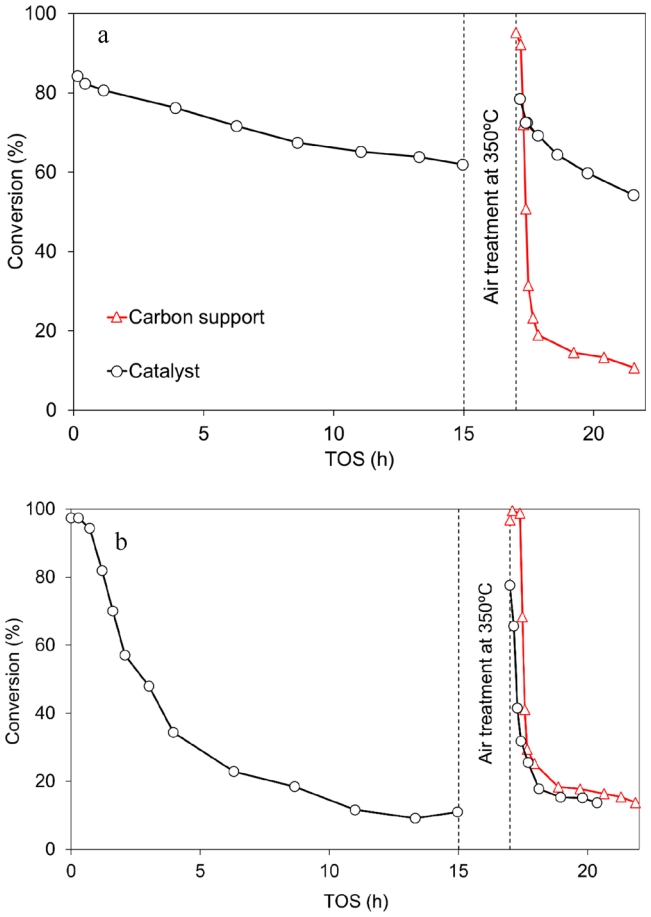

Figure 6. Methanol conversion profiles at (a) 450 °C and (b) 550 °C as a function of TOS of the carbon support and fresh and air-oxidized spent catalysts at a methanol partial pressure of 0.04 atm and a space time of 75 g_{cat} s $mmol_{CH_3OH}^{-1}$.

the surface of this catalyst after reaction under these temperatures: a coke deposited on the C−O−P surface centers of the catalytic support that is oxidizable in air at 350 °C and another type of coke very much resistant to oxidation in air at this temperature treatment deposited on the Zr−O−P active sites of the surface groups of zirconium phosphate of the catalyst. In the case of the air-treated spent catalyst (at 450 °C), the methanol conversion profile can be considered as the sum of the residual conversion associated with zirconium phosphate sites and these new C−O−P surface groups, which means that air treatment only affects the first hours, and then, when the support loses its residual activity, conversion will have the same tendency as that observed for the catalyst without air treatment.

On the other hand, no differences were found regarding the selectivity of methanol toward the different products for the samples before and after reaction at 450 and 550 °C, except for a slightly increase of the selectivity to CH_4 observed for the catalyst deactivated at 550 °C with subsequent treatment in air (higher than 60% at 550 °C), which can be associated with the unsuccessful elimination of coke from zirconium phosphate groups and the appearance of new phosphorus−coke bonds, whose selectivity to methane is quite high.

With this goal, a new experiment was performed (Figure S3 of the Supporting Information) in which the fresh catalyst was used in reaction at 450 °C, with a 4% methanol partial pressure and a space time of 75 g_{cat} s $mmol_{CH_3OH}^{-1}$, at long TOS (70 h). The catalyst showed a relatively high stability at this temperature, with conversion values higher than 40% for 70 h of TOS and very high selectivity to DME (values higher than 90% for the whole range of TOS evaluated) under the operation conditions studied.

For the sake of comparison, a similar experiment at the same operation conditions was carried out with the fresh catalyst (Figure S3 of the Supporting Information), but now the catalyst was submitted to a regeneration process by air treatment at 350 °C for 2 h every 15 h of TOS. It was observed that the catalyst was partially regenerated as a result of the oxidation of coke deposited on C−O−P active sites, transforming the inactive coke deposited (C−P) surface groups into active C−O−P groups. However, the regenerated catalyst follows the same trend as the fresh catalyst (without any regeneration air treatment during the long TOS experiment) after 5 h of reaction in all of the cases as a result of the slow but irreversible deactivation of Zr−O−P active surface groups by deposition of more oxidation-resistant coke that cannot be burned out by the air treatment at 350 °C.

All of these results seem to point out that the negligible gasification of coke deposits on the Zr−O−P surface species of zirconium phosphate of the catalyst was the main cause for the poor catalyst regeneration. However, a change in crystallinity of zirconium phosphate as a result of the high reaction temperature reached could be another possible explanation to the poor regeneration of the catalyst. To assess the influence on activity of a hypothetical change in crystallinity, an experiment in which the sample was subjected to a helium treatment at 550 °C for 15 h was performed. No change in conversion or selectivity was found between the fresh and

Table 2. Textural Parameter Values Extracted from the N_2 Adsorption Isotherm at −196 °C and CO_2 Adsorption Isotherm at 0 °C of Fresh and Deactivated Catalysts after Reaction at 450 and 550 °C for 15 h and the Corresponding Samples after the Oxidative Air Treatment (AT) at a Methanol Partial Pressure of 0.04 atm and a Space Time of 75 g_{cat} s $mmol_{CH_3OH}^{-1}$ and Followed by Air Treatment at 350 °C

	N_2 isotherm					CO_2 isotherm	
sample	A_{BET} (m^2/g)	A_t (m^2/g)	V_{tot} (cm^3/g)	V_{mes} (cm^3/g)	V_t (cm^3/g)	A_{DR} (m^2/g)	V_{DR} (cm^3/g)
fresh	1130	271	0.86	0.42	0.44	476	0.19
fresh + AT	1153	262	0.84	0.38	0.46	446	0.18
450 °C	816	221	0.62	0.32	0.30	290	0.12
450 °C + AT	852	223	0.64	0.32	0.32	348	0.14
550 °C	614	187	0.48	0.27	0.22	242	0.10
550 °C + AT	634	189	0.49	0.27	0.22	273	0.11

https://doi.org/10.1021/acs.energyfuels.1c01721
Energy Fuels 2021, 35, 17225−17240

thermal-treated sample, ruling out the possibility of a change in crystallinity as responsible for catalyst deactivation.

3.5. Characterization of Air-Treated Deactivated Catalysts. N_2 adsorption−desorption isotherms of the partial and almost totally deactivated catalysts at 450 and 550 °C, respectively, followed by the oxidative treatment in air at 350 °C are presented in Figure S4 of the Supporting Information. Their corresponding textural parameters are gathered in Table 2. For the sake of comparison, the N_2 adsorption−desorption isotherm of the fresh catalyst after the oxidative treatment was also included in Figure S4 of the Supporting Information. The mild conditions of the oxidation treatment resulted in minimal differences between the isotherms of the fresh and air-treated catalysts. These results are in concordance with the low burnoff observed for the carbon support and deactivated catalysts (<4%), associated with the high oxidation resistance of the carbon support as a result of the presence of phosphorus groups on the carbon surface.[65]

The isotherms of the catalyst used in the reaction, before and after the oxidation treatment, presented fair similarities, showing only a low increase in the N_2-adsorbed volume at low relative pressures. On the other hand, the results presented in Table 2 show that the oxidative treatment to the fresh catalyst (fresh + AT) led to a slight decrease in the micropore volume measured with CO_2 and the mesopore volume, which also resulted in a reduction in the narrow micropore area and external area, suggesting that the oxidation of C−P bonds of the catalyst carbon support to C−O−P bonds took place mainly on the narrow micropore and external surfaces of the catalyst support. Furthermore, the oxidative treatment of the partially deactivated catalyst after reacting at 450 °C produced a somewhat more significant increase (14%) in the volume of the micropore measured with CO_2 and, to a lesser extent, in the volume of micropore measured with N_2, without any observed modification of the mesopore volume. The effect of the oxidative treatment on the catalyst obtained after reaction at 550 °C was mainly focused on the increase of the narrow micropore, although to a lesser degree. These results indicate that the deposition of coke on the phosphorus species of the catalyst surface, the only type of coke that could be removed from the catalyst under the oxidative treatment conditions, took place to a greater extent on the narrow micropore surface of the catalyst. Nevertheless, none of the values of the different textural parameters obtained for the fresh catalyst could be completely restored by the oxidative treatment in air carried out on the partially and almost totally deactivated catalysts (after reaction at 450 and 550 °C, respectively), which suggest that the zirconium phosphate surface species were very well-dispersed on the whole catalyst surface. The fact that this reduction occurred to a greater extent for the narrow micropores suggests that some of the narrower micropores were blocked, probably as a result of diffusion limitations to these reaction temperatures.

TPD experiments were performed for the fresh and deactivated catalysts before and after the oxidizing treatment (Figure 7). The CO TPD profile for the fresh catalyst showed three main peaks: a CO peak evolving at around 860 °C, which was related to decomposition of C−O−P groups, a peak at around 1000 °C, which was attributed to the decomposition of C−O−Zr bonds present in zirconium phosphate groups linked to the carbon surface, and a CO evolution appearing at around 1300−1350 °C, which was correlated to zirconium−carbon/

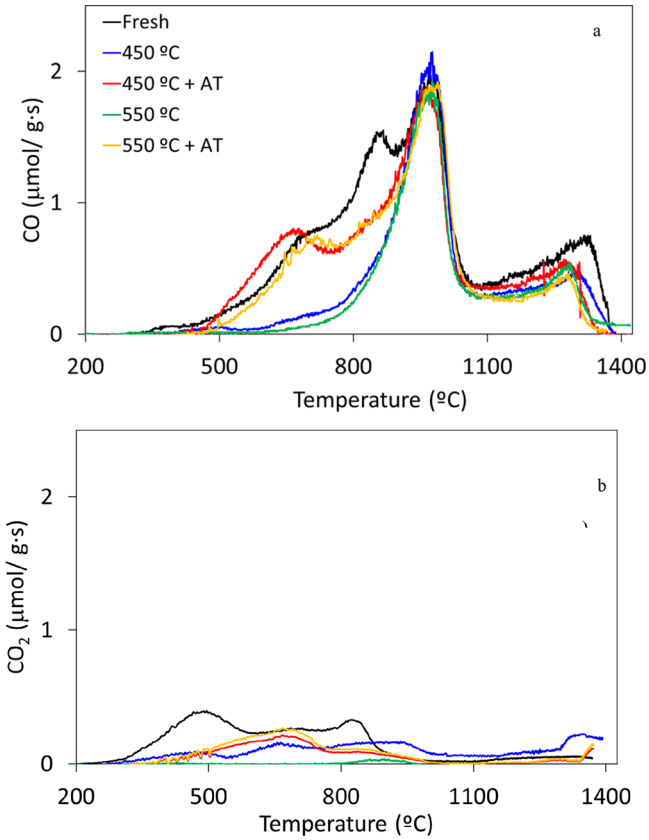

Figure 7. Amount of CO and CO_2 evolved as a function of the temperature during TPD of fresh and used samples and air-oxidized samples at a methanol partial pressure of 0.04 atm and a space time of 75 g_{cat} s $mmol_{CH_3OH}^{-1}$.

ZrO_2 species and/or the ZrO_2 carboreduction, occurring at such a high temperature.[80]

The CO evolution at around 860 °C, associated with the decomposition of C−O−P groups, almost disappeared after reaction at 450 and 550 °C, which could be related to deactivation of these groups by coke deposition, thus reducing the C−O−P bonds to C−P bonds.[74] After the air treatment (AT), only some of these groups were regenerated, suggesting that the complete recovery of the C−O−P groups was not possible presumably because of those groups that were on the surface of the narrower micropores that ended up blocked during the reaction. The CO peak associated with decomposition of zirconium−carbon/ZrO_2 species diminished after reaction and could not be recovered after the oxidative air treatment, showing that the coke layer deposited on these sites was strongly linked. As a consequence of the oxidative air treatment, new carbon−oxygen groups of lower thermal stability, like phenol groups, were produced on the surface of the carbon support, which decomposed as CO at temperatures of around 700 °C. Interestingly, the peak associated with decomposition of C−O−Zr bonds present in zirconium phosphate groups, which in the fresh catalyst was the largest peak, remained practically the same for the profiles of deactivated catalysts and also those of the samples that were treated in air at 350 °C, which indicates the high stability of these bonds compared to that of the C−O−P bonds and that these C−O−Zr surface species were not active for the dehydration of methanol to DME.

https://doi.org/10.1021/acs.energyfuels.1c01721
Energy Fuels 2021, 35, 17225−17240

On the other hand, the CO_2 TPD profile of the fresh catalyst mainly indicated the presence of anhydride groups (decomposed at around 470 °C) and carboxylic acid groups (around 310 °C). However, the intensity of these peaks was much lower than the intensity of CO-evolving groups, which means that their concentrations are considerably lower. Although the formation of the carboxylic groups could be interesting for this reaction as a result of their acid character,[61] they are not stable at temperatures higher than 350 °C.

Surface chemistry of deactivated catalysts was studied by XPS analyses (Table 3). After reaction at 450 and 550 °C, the catalyst surface oxygen, phosphorus, and zirconium concentrations decreased, while the carbon content increased as a result of coke deposition (as mentioned in section 3.3) Oxidative treatment of deactivated catalysts (450 °C + AT and 550 °C + AT) resulted in a decrease of the surface carbon concentration and an increase of phosphorus, zirconium, and especially oxygen concentrations. It is important to highlight that, after the air treatment at 350 °C, the observed surface phosphorus concentration was even higher than that on the fresh catalyst. Some gasification of the carbon support during the removal of deposited coke as well as a migration of phosphorus and zirconium from the internal surface to the external surface could be responsible for this increase.

Table 3. Atomic Surface Concentration by XPS of Fresh and Spent Catalysts after Reaction at Several Temperatures and after Air Treatment at 350 °C at a Methanol Partial Pressure of 0.04 atm and a Space Time of 75 g_{cat} s $mmol_{CH_3OH}^{-1}$

sample	C_{1s}	O_{1s}	P_{2p}	Zr_{3d}	P/Zr	C/P	C/Zr
fresh	61.2	30.5	4.4	3.9	1.1	13.9	15.7
450 °C	78.4	16.1	2.8	2.5	1.1	27.8	31.0
450 °C + AT	49.8	37.5	8.3	4.4	1.9	6.0	11.4
550 °C	86.0	10.5	2.3	1.2	2.0	37.1	72.9
550 °C + AT	57.4	30.9	8.1	3.5	2.3	7.1	16.2

Further information can be obtained from individual XPS spectra. Figure 5 also shows the XPS spectra of Zr_{3d} and P_{2p} of the deactivated catalysts after the air treatment. The P_{2p} spectrum after the air treatment (450 °C + AT) showed an increase of the bands associated with zirconium phosphate as well as C−O−P groups, probably as a result of the migration of these compounds to the external surface and the oxidation of C−P−O groups into C−O−PO groups, in agreement with the results obtained from TPD analysis. Furthermore, a small shift of the bands corresponding to zirconium phosphate surface groups can be observed, which could be related to a higher polarization of the environment.[99] The Zr_{3d} spectrum of the deactivated catalyst (450 °C + AT) showed a maximum of the peak appearing at 184.5 eV, which corresponds to the presence of Zr(IV) bound to an electroactive species, such as phosphorus, in form of a pyrophosphate group, with a higher polarization of the environment (Figure 5b).[99] These results seem to indicate that the −OH group of zirconium phosphate, which was substituted by organic groups (coke), could not be recovered after the air treatment.

With the goal of confirming this hypothesis, ^{31}P NMR spectra of the carbon support, the fresh catalyst, the deactivated catalysts at 450 and 550 °C, and one of the air oxidized samples (450 °C + AT) are presented in Figure 8. Two main peaks can be seen in the spectrum of the carbon support as well as in that of the fresh catalyst. First, a broad band between 20 and −10 ppm was observed, which could be associated with the sum of several species with similar intensities, such as phosphonates, around 20 ppm, and P esters, around 3 ppm.[62,100] In addition, a narrow peak highlighted at −4 ppm appeared, which could be associated with zirconium phosphate species or some P esters, like $Zr(HPO_4)_2{\cdot}H_2O$[101] or $(C{-}O)_x{-}P{-}OH$.[102] The spectrum significantly changed after reaction at 450 and 550 °C, and the broad peak between 20 and −10 ppm, associated with phosphonates and P esters, almost disappeared, as a consequence of coke deposition. These results were in line with the reduction of C−O−P groups after reaction at these temperatures deduced from the TPD analysis and in agreement with the findings reported by Valero-Romero et al.[74]

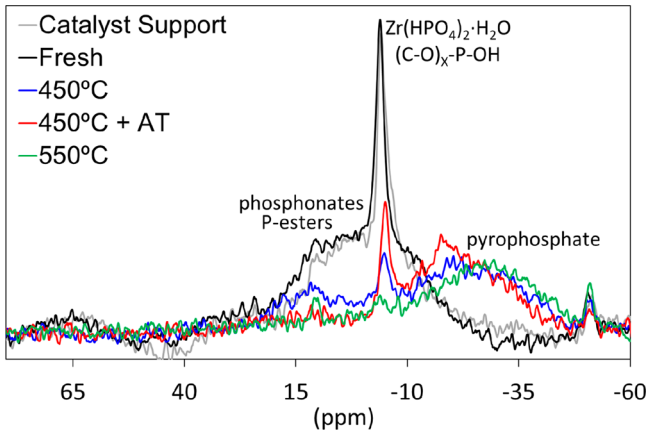

Figure 8. ^{31}P NMR spectra for the carbon support, fresh, partially, and almost totally deactivated catalysts at 450 and 550 °C, respectively, and oxidized sample after reaction at 450 °C at a methanol partial pressure of 0.04 atm and a space time of 75 g_{cat} s $mmol_{CH_3OH}^{-1}$.

For the catalyst used at a reaction temperature of 450 °C, the sharp peak at −4 ppm was considerably reduced and was almost negligible for the catalyst after reaction at 550 °C. It should be noted that the catalyst after reaction at 450 °C maintained some activity for the methanol dehydration reaction. However, after reaction at 550 °C, the catalyst was practically exhausted, suggesting that the zirconium phosphate species was mainly responsible for the high activity of this catalyst. Thus, the peak at −4 ppm observed for the partially deactivated catalyst after reaction at 450 °C could be ascribed to zirconium phosphate species that still remained on the catalyst surface after 15 h of reaction. Nevertheless, the increase observed for this peak for the sample obtained after the air treatment carried out over the catalyst partially deactivated at 450 °C was probably due to the presence of C−O−PO surface groups on the sample, appearing as a consequence of oxidation of C−P−O groups to C−O−PO groups, as also indicated by the results of TPD, and could explain the slight increase observed in conversion of that oxidized sample that was, however, deactivated very fast. This effect was already observed in the P_{2p} XPS spectrum, in which the contribution of C−O−PO groups increased after air treatment of the deactivated catalyst at 450 °C.

On the other hand, the spectra for the samples exposed to reaction at 450 and 550 °C and to the subsequent air treatment showed a peak at around −28 ppm, which can be

https://doi.org/10.1021/acs.energyfuels.1c01721
Energy Fuels 2021, 35, 17225−17240

Scheme 1. Reaction Pathway for the Deactivation of the Catalyst in the MTD Process

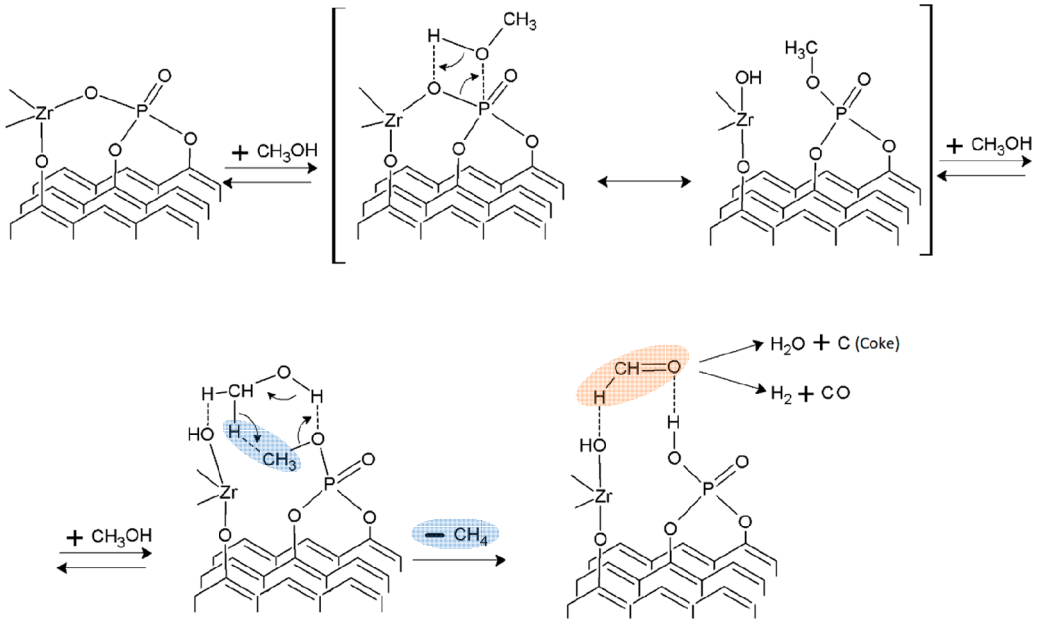

associated with non-hydrogenated phosphate (pyrophosphate)[103,104] or species like P_2O_5.[105] These results seem to indicate that zirconium phosphate surface groups were converted into zirconium pyrophosphate groups under these operation conditions. The formation of zirconium pyrophosphate groups can be related to the residual conversion of these samples for long TOS.

To confirm the above statement, 2D HETCOR $^{31}P-^{1}H$ NMR was also performed in the fresh and partially deactivated catalyst at 450 °C, and results are shown in Figure S5 of the Supporting Information. A clear connection between the peak of phosphorus at −4 ppm and hydrogen was observed for the fresh catalyst, which is associated with phosphate groups containing −OH groups. Nevertheless, after reaction at 550 °C, when the catalyst presented only a residual activity, this interaction between phosphorus and hydrogen cannot be observed, suggesting the consumption of these −OH bonds.

3.6. Reaction Pathway. In a previous paper, a modified Langmuir−Hinshelwood mechanism accounting for two molecules of methanol subsequently on one active site with different adsorption enthalpies and competitive adsorption of water was proposed for the MTD reaction on a similar catalyst at low temperatures (250−350 °C) and low methanol conversions (<50%).[81] This reaction route considered that Zr−O−P active sites of zirconium phosphate surface groups may reversibly adsorb a methanol molecule in a first step, yielding from cleavage of the site a methoxy group bonded to phosphorus and a vicinal −OH bonded to zirconium. In the next step, a second molecule of methanol is reversible adsorbed on generated Zr−OH, reacting with the methoxy group to produce reversibly DME and adsorbed water in form of two hydroxyl groups (Zr−OH and P−OH) in a further stage (step 3). In the last step, the hydroxyl groups react to produce water, regenerating, this way, the initial active site.

In this work, on the basis of the experimental catalytic results obtained at a higher temperature and the characterization of the catalysts used in the reaction, a modified reaction pathway has been proposed, which explains the coke production and deactivation of the catalyst. The higher DME production observed at reaction temperatures of above 400 °C could lead to a greater stability of the adsorbed DME species, favoring now an irreversible process (see Scheme 1), leading to the formation of methane and adsorbed formaldehyde on the active center. The latter is considered an intermediate product in the production of H_2 and CO and in the formation of coke on the active centers, with water vapor releasing. This would explain the appearance of small amounts of H_2 and CO in the reaction products and the presence of coke and excess of water observed with an increasing reaction temperature. Once the catalyst was partially deactivated, the concentration of DME in the gas phase decreased, increasing that of methanol. In this case, the production of coke could also occur through the formation of methoxy species on the active centers of the catalyst (Zr−O−P and/or Zr−OH and P−OH), preventing their regeneration in the reaction.

Ruiz-Rosas et al.[106] reported that Zr−OH species were active for methanol decomposition above 450 °C, although these species were deactivated by coke deposition. Thus, hydroxyl bonded to zirconium can irreversibly interact with methanol, releasing water and letting a methoxy group bond to zirconium. In this sense, XPS results also pointed out that the zirconium atomic concentration was first decreased during the reaction, suggesting that the formation of methoxy groups and the consequent growth of coke could be responsible for this decrease. On the other hand, the rapid deactivation of P−OH and C−O−P groups at temperatures even lower than those used in the present study has already been reported in the literature.[74] Cheng et al. also indicated that P−methoxy species ($P-CH_3$) formed by reaction of methanol on zirconium phosphate catalysts can react with a second methanol molecule through a six-member-ring electron transfer process to irreversibly produce methane and formaldehyde. These findings also support the reaction scheme proposed in this work (see Scheme 1) that accounts for the gas product distribution and the production of coke that generates the deactivation of the catalysts.

3.7. Kinetic Analysis of Coke Deposition. Finally, to predict the coke formation experimental results, a kinetic

https://doi.org/10.1021/acs.energyfuels.1c01721
Energy Fuels 2021, 35, 17225−17240

model initially proposed by Froment, Bischoff, and De Wilde was used.[107] With this goal, the coke content of the catalyst at different reaction temperatures and TOS was quantified. The kinetic model takes into account a deactivation function, which depends upon the coke content

$$\frac{dC_C}{dt} = r_C^0 \Phi_C \tag{3}$$

$$\Phi_C = (1 - \alpha C_C)^2 \tag{4}$$

where C_C is the percentage of coke deposited, t is the TOS, r_C^0 is the initial rate of coke production, Φ_C is the deactivation function, and α is the deactivation factor. Assuming differential conditions for coke production, the integrated equation takes the form

$$C_C = \frac{1}{\alpha}\left[1 - \frac{1}{1 + \alpha r_C^0 t}\right] \tag{5}$$

where r_C^0 and α are the fitting parameters. It should be pointed out that α is considered to be constant in all of the experiments.[107] The fitting parameters were calculated using a Nelder–Mead simplex algorithm, which minimizes the objective function (eq 6), defined as the sum of quadratic differences between the experimental coke content and the calculated values

$$\mathrm{OF} = \sum_{i=1}^{n_T} (C_{i,\mathrm{exp}} - C_{i,\mathrm{cal}})^2 \tag{6}$$

where n_T is the total number of experiments and $C_{i,\mathrm{exp}}$ and $C_{i,\mathrm{cal}}$ are the experimental and calculated coke contents of the ith experiment, respectively.

The initial rate of coke formation, r_C^0, obtained at different temperatures, can be defined as a simple n-order power law equation and used to obtain the activation energy of the coke formation

$$r_C^0 = k P_{CH_3OH}^n \tag{7}$$

where $P_{CH_3OH}^n$ is the fed partial pressure of methanol and k is a kinetic constant that follows the Arrhenius law

$$r_C^0 = k_0 e^{-E_a/RT} P_{CH_3OH}^n = k_0' e^{-E_a/RT} \tag{8}$$

where k_0 is the pre-exponential factor, k_0' is the apparent pre-exponential factor, E_a is the activation energy, R is the ideal gas constant, and T is the reaction temperature. In these experiments, the partial pressure of methanol was maintained at 0.04 atm.

The amount of coke deposited on the catalyst as a function of TOS for different reaction temperatures is represented in Figure 9. The content of coke deposited on the catalyst and the rate of coke formation increased with TOS and reaction temperature. However, a somewhat saturation level could be observed in the final content of coke deposited on the catalyst with an increasing temperature, with a value close to 25%. This behavior could be related to the greater reduction of the narrow microporosity observed with the increase in the reaction rate, probably leaving part of the narrow micropores closed during the process at the highest reaction temperatures. Kinetic parameters are summarized in Table 4. The activation energy value obtained for coke formation was 124 kJ/mol, slightly higher than the activation energies reported for other catalysts at similar experimental conditions.[86,108,109] Experimental and calculated coke contents are represented in Figure 9, showing good agreement between both values.

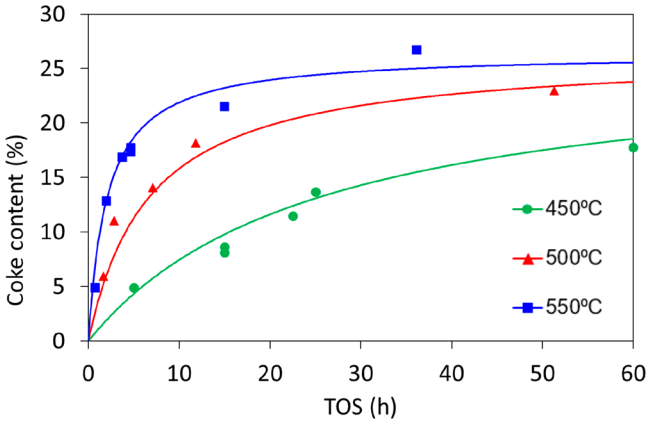

Figure 9. Experimental (points) and calculated (lines) coke contents as a function of TOS at different reaction temperatures at a methanol partial pressure of 0.04 atm and a space time of 75 g_{cat} s $mmol_{CH_3OH}^{-1}$.

Table 4. Coke Formation Kinetic Parameters

kinetic parameter	value
deactivation constant, α	0.038
coking activation energy, E_a (kJ/mol)	124
apparent pre-exponential factor, k_0'	9.5×10^8
R^2	0.97

4. CONCLUSION

Dehydration of methanol to produce DME was studied at different temperatures (300–600 °C) on a biomass-derived phosphorus-containing carbon impregnated with a zirconium salt. Highly thermally stable zirconium phosphate surface groups could be obtained on the final catalyst, which were responsible for the high stability and selectivity to DME of the catalyst at temperatures lower than 450 °C. However, harder operation conditions, closer to those of the industrial process, were evaluated to analyze the changes of the catalyst surface properties with the reaction temperature and the possible causes of deactivation. Thus, high methanol conversion and selectivity to DME were also observed for this biomass-derived catalyst in the temperature range of 450–600 °C, although deactivation was observed. Coke deposition was responsible for a decrease in microporosity and surface concentration of zirconium and phosphorus of the catalyst. TPD, ^{31}P MAS NMR, and XPS results suggest that the Zr–O–P groups from zirconium phosphate species were responsible for the long-term stability of the catalyst and that the C–O–P-type active sites deactivated very fast. However, coke deposition on Zr–O–P-type active sites during the reaction caused a slow and irreversible deactivation, given that removal of the deposited coke from these active sites by gasification in air at 350 °C proved to be very difficult. Nevertheless, a different nature of deposited coke took place on the C–O–P-type active sites, which was easily eliminated by the oxidative treatment in air. A reaction scheme that accounted for the gas product distribution and the production of coke that generated the deactivation of the catalysts was postulated. A kinetic model for coke formation as a function of TOS that successfully represent the experimental results was also proposed, which

https://doi.org/10.1021/acs.energyfuels.1c01721
Energy Fuels 2021, 35, 17225–17240

yielded a value for the activation energy for the production of coke of 124 kJ/mol.

■ ASSOCIATED CONTENT

Supporting Information

The Supporting Information is available free of charge at https://pubs.acs.org/doi/10.1021/acs.energyfuels.1c01721.

Atomic surface concentration (%) obtained by XPS of fresh and spent catalysts with different coke contents for a reaction temperature of 500 °C and different TOS at a methanol partial pressure of 0.04 atm and a space time of 75 g_{cat} s $mmol_{CH_3OH}^{-1}$ (Table S1), pore size distribution of fresh and spent catalysts with the same coke content (18%) obtained at different reaction temperatures and TOS at a methanol partial pressure of 0.04 atm and a space time of 75 g_{cat} s $mmol_{CH_3OH}^{-1}$ (Figure S1), pore size distribution of fresh and spent catalysts at the same reaction temperature (500 °C) obtained at different reaction TOS and with different coke contents at a methanol partial pressure of 0.04 atm and a space time of 75 g_{cat} s $mmol_{CH_3OH}^{-1}$ (Figure S2), (a) methanol conversion profile as a function of TOS for long-term experiment and for consecutive cycles of reaction air treatment and (b) selectivity for long-term experiment, with reaction conditions of 450 °C at a methanol partial pressure of 0.04 atm and a space time of 75 g_{cat} s $mmol_{CH_3OH}^{-1}$ and air treatment conditions of 350 °C for 2 h (Figure S3), N_2 adsorption−desorption isotherms at −196 °C of fresh and spent catalysts at 450 and 550 °C for 15 h at a methanol partial pressure of 0.04 atm and a space time of 75 g_{cat} s $mmol_{CH_3OH}^{-1}$ and the same samples after air treatment (Figure S4), and 2D HETCOR $^{31}P-^{1}H$ NMR of (a) fresh and (b) spent catalysts after reaction at 550 °C for 15 h at a methanol partial pressure of 0.04 atm and a space time of 75 g_{cat} s $mmol_{CH_3OH}^{-1}$ (Figure S5) (PDF)

■ AUTHOR INFORMATION

Corresponding Author

Tomás Cordero − *Andalucía Tech, Departamento de Ingeniería Química, Universidad de Málaga, 29010 Málaga, Spain;* orcid.org/0000-0002-3557-881X; Email: cordero@uma.es

Authors

Javier Torres-Liñán − *Andalucía Tech, Departamento de Ingeniería Química, Universidad de Málaga, 29010 Málaga, Spain;* orcid.org/0000-0002-6733-895X

Miguel García-Rollán − *Andalucía Tech, Departamento de Ingeniería Química, Universidad de Málaga, 29010 Málaga, Spain*

Juana M. Rosas − *Andalucía Tech, Departamento de Ingeniería Química, Universidad de Málaga, 29010 Málaga, Spain;* orcid.org/0000-0001-9158-3413

José Rodríguez-Mirasol − *Andalucía Tech, Departamento de Ingeniería Química, Universidad de Málaga, 29010 Málaga, Spain;* orcid.org/0000-0003-3122-1220

Complete contact information is available at: https://pubs.acs.org/10.1021/acs.energyfuels.1c01721

Notes

The authors declare no competing financial interest.

■ ACKNOWLEDGMENTS

This work was supported by the Spanish Ministry of Economy and Competitiveness and Junta de Andalucia through CTQ2015-68654-R, RTI2018-097555-B-I00, and UMA18-FEDERJA-110 projects. Javier Torres-Liñán also acknowledges the assistance of the Spanish Ministry of Economy, Industry and Competitiveness for the award of a predoctoral contract to become a Ph.D. (BES-2016-079237).

■ REFERENCES

(1) Meinshausen, M.; Meinshausen, N.; Hare, W.; Raper, S. C. B.; Frieler, K.; Knutti, R.; Frame, D. J.; Allen, M. R. Greenhouse-Gas Emission Targets for Limiting Global Warming to 2 °C. *Nature* **2009**, *458* (7242), 1158−1162.

(2) Hansen, J.; Sato, M.; Ruedy, R.; Lacis, A.; Oinas, V. Global Warming in the Twenty-First Century: An Alternative Scenario. *Proc. Natl. Acad. Sci. U. S. A.* **2000**, *97* (18), 9875−9880.

(3) McGlade, C.; Ekins, P. The Geographical Distribution of Fossil Fuels Unused When Limiting Global Warming to 2 °C. *Nature* **2015**, *517* (7533), 187−190.

(4) Omer, A. M. Energy, Environment and Sustainable Development. *Renewable Sustainable Energy Rev.* **2008**, *12* (9), 2265−2300.

(5) United Nations General Assembly. *Transforming Our World: The 2030 Agenda for Sustainable Development*; United Nations General Assembly: New York, Sept 25, 2015.

(6) Rodríguez, E.; Palos, R.; Gutiérrez, A.; Trueba, D.; Arandes, J. M.; Bilbao, J. Towards Waste Refinery: Co-Feeding HDPE Pyrolysis Waxes with VGO into the Catalytic Cracking Unit. *Energy Convers. Manage.* **2020**, *207*, 112554.

(7) Palos, R.; Gutiérrez, A.; Vela, F. J.; Olazar, M.; Arandes, J. M.; Bilbao, J. Waste Refinery: The Valorization of Waste Plastics and End-of-Life Tires in Refinery Units. A Review. *Energy Fuels* **2021**, *35* (5), 3529−3557.

(8) De Bhowmick, G.; Sarmah, A. K.; Sen, R. Lignocellulosic Biorefinery as a Model for Sustainable Development of Biofuels and Value Added Products. *Bioresour. Technol.* **2018**, *247*, 1144−1154.

(9) FitzPatrick, M.; Champagne, P.; Cunningham, M. F.; Whitney, R. A. A Biorefinery Processing Perspective: Treatment of Lignocellulosic Materials for the Production of Value-Added Products. *Bioresour. Technol.* **2010**, *101* (23), 8915−8922.

(10) Parajuli, R.; Dalgaard, T.; Jørgensen, U.; Adamsen, A. P. S.; Knudsen, M. T.; Birkved, M.; Gylling, M.; Schjørring, J. K. Biorefining in the Prevailing Energy and Materials Crisis: A Review of Sustainable Pathways for Biorefinery Value Chains and Sustainability Assessment Methodologies. *Renewable Sustainable Energy Rev.* **2015**, *43*, 244−263.

(11) Takkellapati, S.; Li, T.; Gonzalez, M. A. An Overview of Biorefinery-Derived Platform Chemicals from a Cellulose and Hemicellulose Biorefinery. *Clean Technol. Environ. Policy* **2018**, *20* (7), 1615−1630.

(12) Arcoumanis, C.; Bae, C.; Crookes, R.; Kinoshita, E. The Potential of Di-Methyl Ether (DME) as an Alternative Fuel for Compression-Ignition Engines: A Review. *Fuel* **2008**, *87* (7), 1014−1030.

(13) Park, S. H.; Lee, C. S. Applicability of Dimethyl Ether (DME) in a Compression Ignition Engine as an Alternative Fuel. *Energy Convers. Manage.* **2014**, *86*, 848−863.

(14) Anggarani, R.; Wibowo, C. S.; Rulianto, D. Application of Dimethyl Ether as LPG Substitution for Household Stove. *Energy Procedia* **2014**, *47*, 227−234.

(15) Li, J.; Zhang, Q.; Zhao, Y.; Qi, P.; Shao, C. Alkaline Earth Metal Oxide Modification of Ni/Al_2O_3 for Hydrogen Production from the Partial Oxidation and Reforming of Dimethyl Ether. *React. Kinet., Mech. Catal.* **2017**, *122*, 1193−1202.

(16) Kim, D.; Park, G.; Choi, B.; Kim, Y. B. Reaction Characteristics of Dimethyl Ether (DME) Steam Reforming Catalysts for Hydrogen Production. *Int. J. Hydrogen Energy* **2017**, *42* (49), 29210−29221.
(17) Saravanan, K.; Ham, H.; Tsubaki, N.; Bae, J. W. Recent Progress for Direct Synthesis of Dimethyl Ether from Syngas on the Heterogeneous Bifunctional Hybrid Catalysts. *Appl. Catal., B* **2017**, *217*, 494−522.
(18) Haro, P.; Trippe, F.; Stahl, R.; Henrich, E. Bio-Syngas to Gasoline and Olefins via DME—A Comprehensive Techno-Economic Assessment. *Appl. Energy* **2013**, *108*, 54−65.
(19) Hajjar, Z.; Khodadadi, A.; Mortazavi, Y.; Tayyebi, S.; Soltanali, S. Artificial Intelligence Modeling of DME Conversion to Gasoline and Light Olefins over Modified Nano ZSM-5 Catalysts. *Fuel* **2016**, *179*, 79−86.
(20) Zhou, H.; Wang, Y.; Wei, F.; Wang, D.; Wang, Z. In Situ Synthesis of SAPO-34 Crystals Grown onto α-Al_2O_3 Sphere Supports as the Catalyst for the Fluidized Bed Conversion of Dimethyl Ether to Olefins. *Appl. Catal., A* **2008**, *341* (1−2), 112−118.
(21) Ortega, C.; Hessel, V.; Kolb, G. Dimethyl Ether to Hydrocarbons over ZSM-5: Kinetic Study in an External Recycle Reactor. *Chem. Eng. J.* **2018**, *354*, 21−34.
(22) Mordor Intelligence. *Dimethyl Ether (DME) Market—Growth, Trends, COVID-19 Impact, and Forecasts (2021−2026)*; Mordor Intelligence: Hyderabad, India, 2021; https://www.mordorintelligence.com/industry-reports/dimethyl-ether-market (accessed May 31, 2021).
(23) *Methanol: The Basic Chemical and Energy Feedstock of the Future: Asinger's Vision Today*; Bertau, M., Offermanns, H., Plass, L., Schmidt, F., Wernicke, H.-J., Eds.; Springer: Berlin, Germany, 2014; DOI: 10.1007/978-3-642-39709-7.
(24) Akarmazyan, S. S.; Panagiotopoulou, P.; Kambolis, A.; Papadopoulou, C.; Kondarides, D. I. Methanol Dehydration to Dimethylether over Al_2O_3catalysts. *Appl. Catal., B* **2014**, *145*, 136−148.
(25) Forester, T. R.; Howe, R. F. In Situ FTIR Studies of Methanol and Dimethyl Ether in ZSM-5. *J. Am. Chem. Soc.* **1987**, *109* (17), 5076−5082.
(26) Kim, S.; Kim, Y. T.; Zhang, C.; Kwak, G.; Jun, K.-W. Effect of Reaction Conditions on the Catalytic Dehydration of Methanol to Dimethyl Ether Over a K-Modified HZSM-5 Catalyst. *Catal. Lett.* **2017**, *147* (3), 792−801.
(27) Sierra, I.; Ereña, J.; Aguayo, A. T.; Ateka, A.; Bilbao, J. Kinetic Modelling for the Dehydration of Methanol to Dimethyl Ether over γ-Al_2O_3. *Chem. Eng. Trans.* **2013**, *32*, 613−618.
(28) Guisnet, M.; Magnoux, P. Coking and Deactivation of Zeolites. Influence of the Pore Structure. *Appl. Catal.* **1989**, *54* (1), 1−27.
(29) Müller, S.; Liu, Y.; Vishnuvarthan, M.; Sun, X.; Van Veen, A. C.; Haller, G. L.; Sanchez-Sanchez, M.; Lercher, J. A. Coke Formation and Deactivation Pathways on H-ZSM-5 in the Conversion of Methanol to Olefins. *J. Catal.* **2015**, *325*, 48−59.
(30) Fu, Y.; Hong, T.; Chen, J.; Auroux, A.; Shen, J. Surface Acidity and the Dehydration of Methanol to Dimethyl Ether. *Thermochim. Acta* **2005**, *434* (1−2), 22−26.
(31) Aguayo, T.; Gayubo, A. G.; Vivanco, R.; Olazar, M.; Bilbao, J. Role of Acidity and Microporous Structure in Alternative Catalysts for the Transformation of Methanol into Olefins. *Appl. Catal., A* **2005**, *283*, 197−207.
(32) Azizi, Z.; Rezaeimanesh, M.; Tohidian, T.; Rahimpour, M. R. Dimethyl Ether: A Review of Technologies and Production Challenges. *Chem. Eng. Process.* **2014**, *82*, 150−172.
(33) Ren, S.; Fan, X.; Shang, Z.; Shoemaker, W. R.; Ma, L.; Wu, T.; Li, S.; Klinghoffer, N. B.; Yu, M.; Liang, X. Enhanced Catalytic Performance of Zr Modified CuO/ZnO/Al_2O_3 Catalyst for Methanol and DME Synthesis via CO_2 Hydrogenation. *J. CO2 Util.* **2020**, *36*, 82−95.
(34) Fan, X.; Jin, B.; Ren, S.; Li, S.; Yu, M.; Liang, X. Roles of Interaction between Components in CZZA/HZSM-5 Catalyst for Dimethyl Ether Synthesis via CO_2 Hydrogenation. *AIChE J.* **2021**, e17353.
(35) Lopez, G.; Artetxe, M.; Amutio, M.; Alvarez, J.; Bilbao, J.; Olazar, M. Recent Advances in the Gasification of Waste Plastics. A Critical Overview. *Renewable Sustainable Energy Rev.* **2018**, *82*, 576−596.
(36) Lee, U.; Chung, J. N.; Ingley, H. A. High-Temperature Steam Gasification of Municipal Solid Waste, Rubber, Plastic and Wood. *Energy Fuels* **2014**, *28* (7), 4573−4587.
(37) Brachi, P.; Chirone, R.; Miccio, F.; Miccio, M.; Picarelli, A.; Ruoppolo, G. Fluidized Bed Co-Gasification of Biomass and Polymeric Wastes for a Flexible End-Use of the Syngas: Focus on Bio-Methanol. *Fuel* **2014**, *128*, 88−98.
(38) Belgiorno, V.; De Feo, G.; Della Rocca, C.; Napoli, R. M. A. Energy from Gasification of Solid Wastes. *Waste Manage.* **2003**, *23* (1), 1−15.
(39) Aguayo, A. T.; Ereña, J.; Sierra, I.; Olazar, M.; Bilbao, J. Deactivation and Regeneration of Hybrid Catalysts in the Single-Step Synthesis of Dimethyl Ether from Syngas and CO_2. *Catal. Today* **2005**, *106* (1−4), 265−270.
(40) Sierra, I.; Ereña, J.; Aguayo, A. T.; Arandes, J. M.; Bilbao, J. Regeneration of CuO-ZnO-Al_2O_3/γ-Al_2O_3 Catalyst in the Direct Synthesis of Dimethyl Ether. *Appl. Catal., B* **2010**, *94* (1−2), 108−116.
(41) Sierra, I.; Ereña, J.; Aguayo, A. T.; Arandes, J. M.; Olazar, M.; Bilbao, J. Co-Feeding Water to Attenuate Deactivation of the Catalyst Metallic Function (CuO-ZnO-Al_2O_3) by Coke in the Direct Synthesis of Dimethyl Ether. *Appl. Catal., B* **2011**, *106* (1−2), 167−173.
(42) Ereña, J.; Garoña, R.; Arandes, J. M.; Aguayo, A. T.; Bilbao, J. Effect of Operating Conditions on the Synthesis of Dimethyl Ether over a CuO-ZnO-Al_2O_3/NaHZSM-5 Bifunctional Catalyst. *Catal. Today* **2005**, *107−108*, 467−473.
(43) Ateka, A.; Sierra, I.; Ereña, J.; Bilbao, J.; Aguayo, A. T. Performance of CuO−ZnO−ZrO_2 and CuO−ZnO−MnO as Metallic Functions and SAPO-18 as Acid Function of the Catalyst for the Synthesis of DME Co-Feeding CO_2. *Fuel Process. Technol.* **2016**, *152*, 34−45.
(44) Sánchez-Contador, M.; Ateka, A.; Aguayo, A. T.; Bilbao, J. Direct Synthesis of Dimethyl Ether from CO and CO_2 over a Core-Shell Structured CuO-ZnO-ZrO_2@SAPO-11 Catalyst. *Fuel Process. Technol.* **2018**, *179*, 258−268.
(45) Aguayo, A. T.; Ereña, J.; Mier, D.; Arandes, J. M.; Olazar, M.; Bilbao, J. Kinetic Modeling of Dimethyl Ether Synthesis in a Single Step on a CuO-ZnO-Al_2O_3/γ-Al_2O_3 Catalyst. *Ind. Eng. Chem. Res.* **2007**, *46* (17), 5522−5530.
(46) Ereña, J.; Sierra, I.; Aguayo, A. T.; Ateka, A.; Olazar, M.; Bilbao, J. Kinetic Modelling of Dimethyl Ether Synthesis from (H_2+CO_2) by Considering Catalyst Deactivation. *Chem. Eng. J.* **2011**, *174* (2−3), 660−667.
(47) Pérez-Uriarte, P.; Ateka, A.; Aguayo, A. T.; Gayubo, A. G.; Bilbao, J. Kinetic Model for the Reaction of DME to Olefins over a HZSM-5 Zeolite Catalyst. *Chem. Eng. J.* **2016**, *302*, 801−810.
(48) Diban, N.; Urtiaga, A. M.; Ortiz, I.; Ereña, J.; Bilbao, J.; Aguayo, A. T. Influence of the Membrane Properties on the Catalytic Production of Dimethyl Ether with in Situ Water Removal for the Successful Capture of CO_2. *Chem. Eng. J.* **2013**, *234*, 140−148.
(49) Rodriguez-Vega, P.; Ateka, A.; Kumakiri, I.; Vicente, H.; Ereña, J.; Aguayo, A. T.; Bilbao, J. Experimental Implementation of a Catalytic Membrane Reactor for the Direct Synthesis of DME from H_2+CO/CO_2. *Chem. Eng. Sci.* **2021**, *234*, 116396.
(50) Vicente, J.; Gayubo, A. G.; Ereña, J.; Aguayo, A. T.; Olazar, M.; Bilbao, J. Improving the DME Steam Reforming Catalyst by Alkaline Treatment of the HZSM-5 Zeolite. *Appl. Catal., B* **2013**, *130−131*, 73−83.
(51) Ereña, J.; Vicente, J.; Aguayo, A. T.; Olazar, M.; Bilbao, J.; Gayubo, A. G. Kinetic Behaviour of Catalysts with Different CuO-ZnO-Al_2O_3 Metallic Function Compositions in DME Steam Reforming in a Fluidized Bed. *Appl. Catal., B* **2013**, *142−143*, 315−322.
(52) Pérez-Uriarte, P.; Gamero, M.; Ateka, A.; Díaz, M.; Aguayo, A. T.; Bilbao, J. Effect of the Acidity of HZSM-5 Zeolite and the Binder

in the DME Transformation to Olefins. *Ind. Eng. Chem. Res.* **2016**, *55* (6), 1513−1521.
(53) Pérez-Uriarte, P.; Ateka, A.; Gamero, M.; Aguayo, A. T.; Bilbao, J. Effect of the Operating Conditions in the Transformation of DME to Olefins over a HZSM-5 Zeolite Catalyst. *Ind. Eng. Chem. Res.* **2016**, *55* (23), 6569−6578.
(54) Gayubo, A. G.; Vicente, J.; Ereña, J.; Oar-Arteta, L.; Azkoiti, M. J.; Olazar, M.; Bilbao, J. Causes of Deactivation of Bifunctional Catalysts Made up of CuO-ZnO-Al_2O_3 and Desilicated HZSM-5 Zeolite in DME Steam Reforming. *Appl. Catal., A* **2014**, *483*, 76−84.
(55) Cordero-Lanzac, T.; Aguayo, A. T.; Gayubo, A. G.; Castaño, P.; Bilbao, J. Simultaneous Modeling of the Kinetics for N-Pentane Cracking and the Deactivation of a HZSM-5 Based Catalyst. *Chem. Eng. J.* **2018**, *331*, 818−830.
(56) Cordero-Lanzac, T.; Aguayo, A. T.; Gayubo, A. G.; Castaño, P.; Bilbao, J. A Comprehensive Approach for Designing Different Configurations of Isothermal Reactors with Fast Catalyst Deactivation. *Chem. Eng. J.* **2020**, *379*, 122260.
(57) Cordero-Lanzac, T.; Hita, I.; García-Mateos, F. J.; Castaño, P.; Rodríguez-Mirasol, J.; Cordero, T.; Bilbao, J. Adaptable Kinetic Model for the Transient and Pseudo-Steady States in the Hydrodeoxygenation of Raw Bio-Oil. *Chem. Eng. J.* **2020**, *400*, 124679.
(58) De, S.; Balu, A. M.; Van Der Waal, J. C.; Luque, R. Biomass-Derived Porous Carbon Materials: Synthesis and Catalytic Applications. *ChemCatChem* **2015**, *7* (11), 1608−1629.
(59) Lee, J.; Kim, K. H.; Kwon, E. E. Biochar as a Catalyst. *Renewable Sustainable Energy Rev.* **2017**, *77*, 70−79.
(60) Lam, E.; Luong, J. H. T. Carbon Materials as Catalyst Supports and Catalysts in the Transformation of Biomass to Fuels and Chemicals. *ACS Catal.* **2014**, *4* (10), 3393−3410.
(61) Moreno-Castilla, C.; Carrasco-Marín, F.; Parejo-Pérez, C.; López Ramón, M. V. Dehydration of Methanol to Dimethyl Ether Catalyzed by Oxidized Activated Carbons with Varying Surface Acidic Character. *Carbon* **2001**, *39* (6), 869−875.
(62) Puziy, A. M.; Poddubnaya, O. I.; Socha, R. P.; Gurgul, J.; Wisniewski, M. XPS and NMR Studies of Phosphoric Acid Activated Carbons. *Carbon* **2008**, *46*, 2113−2123.
(63) Molina-Sabio, M.; Rodríguez-Reinoso, F.; Caturla, F.; Sellés, M. J. Porosity in Granular Carbons Activated with Phosphoric Acid. *Carbon* **1995**, *33* (8), 1105−1113.
(64) Bedia, J.; Rosas, J. M.; Márquez, J.; Rodríguez-Mirasol, J.; Cordero, T. Preparation and Characterization of Carbon Based Acid Catalysts for the Dehydration of 2-Propanol. *Carbon* **2009**, *47* (1), 286−294.
(65) Rosas, J. M.; Ruiz-Rosas, R.; Rodríguez-Mirasol, J.; Cordero, T. Kinetic Study of the Oxidation Resistance of Phosphorus-Containing Activated Carbons. *Carbon* **2012**, *50* (4), 1523−1537.
(66) Rosas, J. M.; Bedia, J.; Rodríguez-Mirasol, J.; Cordero, T. HEMP-Derived Activated Carbon Fibers by Chemical Activation with Phosphoric Acid. *Fuel* **2009**, *88* (1), 19−26.
(67) Cordero-Lanzac, T.; Palos, R.; Arandes, J. M.; Castaño, P.; Rodríguez-Mirasol, J.; Cordero, T.; Bilbao, J. Stability of an Acid Activated Carbon Based Bifunctional Catalyst for the Raw Bio-Oil Hydrodeoxygenation. *Appl. Catal., B* **2017**, *203*, 389−399.
(68) Rosas, J. M.; Rodríguez-Mirasol, J.; Cordero, T. NO Reduction on Carbon-Supported Chromium Catalysts. *Energy Fuels* **2010**, *24* (6), 3321−3328.
(69) Bedia, J.; Rosas, J. M.; Rodríguez-Mirasol, J.; Cordero, T. Pd Supported on Mesoporous Activated Carbons with High Oxidation Resistance as Catalysts for Toluene Oxidation. *Appl. Catal., B* **2010**, *94* (1), 8−18.
(70) Hita, I.; Cordero-Lanzac, T.; Gallardo, A.; Arandes, J. M.; Rodríguez-Mirasol, J.; Bilbao, J.; Cordero, T.; Castaño, P. Phosphorus-Containing Activated Carbon as Acid Support in a Bifunctional Pt-Pd Catalyst for Tire Oil Hydrocracking. *Catal. Commun.* **2016**, *78*, 48−51.
(71) Bedia, J.; Ruiz-Rosas, R.; Rodríguez-Mirasol, J.; Cordero, T. A Kinetic Study of 2-Propanol Dehydration on Carbon Acid Catalysts. *J. Catal.* **2010**, *271* (1), 33−42.
(72) Bedia, J.; Barrionuevo, R.; Rodríguez-Mirasol, J.; Cordero, T. Ethanol Dehydration to Ethylene on Acid Carbon Catalysts. *Appl. Catal., B* **2011**, *103*, 302−310.
(73) Soto, J.; Rosas, J. M.; Otero, J. C.; Rodríguez-Mirasol, J.; Cordero, T. Reaction Mechanisms of 2-Butanol Dehydration over a Phosphorus-Containing Activated Carbon Acid Catalyst. *J. Phys. Chem. C* **2018**, *122* (29), 16772−16778.
(74) Valero-Romero, M. J.; Calvo-Muñoz, E. M.; Ruiz-Rosas, R.; Rodríguez-Mirasol, J.; Cordero, T. Phosphorus-Containing Mesoporous Carbon Acid Catalyst for Methanol Dehydration to Dimethyl Ether. *Ind. Eng. Chem. Res.* **2019**, *58*, 4042−4053.
(75) Nozaki, F.; Itoh, T.; Ueda, S. Catalytic Activity of Zirconium Phosphate for Dehydration of 2-Propanol. *Nippon Kagaku Kaishi* **1973**, *1973* (4), 674−678.
(76) Johnstone, R. A. W.; Liu, J.; Whittaker, D. Mechanism of Cyclohexanol Dehydration Catalysed by Zirconium Phosphate. *J. Chem. Soc., Perkin Trans. 2* **1998**, *0* (6), 1287−1288.
(77) Cheng, L.; Guo, X.; Song, C.; Yu, G.; Cui, Y.; Xue, N.; Peng, L.; Guo, X.; Ding, W. High Performance Mesoporous Zirconium Phosphate for Dehydration of Xylose to Furfural in Aqueous-Phase. *RSC Adv.* **2013**, *3* (45), 23228−23235.
(78) Ni, W.; Li, D.; Zhao, X.; Ma, W.; Kong, K.; Gu, Q.; Chen, M.; Hou, Z. Catalytic Dehydration of Sorbitol and Fructose by Acid-Modified Zirconium Phosphate. *Catal. Today* **2019**, *319*, 66−75.
(79) Cheng, S.; Peng, G. Z.; Clearfield, A. Decomposition of Alcohols over Zirconium and Titanium Phosphates. *Ind. Eng. Chem. Prod. Res. Dev.* **1984**, *23* (2), 219−225.
(80) Palomo, J.; Rodríguez-Mirasol, J.; Cordero, T. Methanol Dehydration to Dimethyl Ether on Zr-Loaded P-Containing Mesoporous Activated Carbon Catalysts. *Materials* **2019**, *12* (13), 2204.
(81) Palomo, J.; Rodríguez-Cano, M. A.; Rodríguez-Mirasol, J.; Cordero, T. On the Kinetics of Methanol Dehydration to Dimethyl Ether on Zr-Loaded P-Containing Mesoporous Activated Carbon Catalyst. *Chem. Eng. J.* **2019**, *378*, 122198.
(82) Alharbi, W.; Kozhevnikova, E. F.; Kozhevnikov, I. V. Dehydration of Methanol to Dimethyl Ether over Heteropoly Acid Catalysts: The Relationship between Reaction Rate and Catalyst Acid Strength. *ACS Catal.* **2015**, *5* (12), 7186−7193.
(83) Janssens, T. V. W. A New Approach to the Modeling of Deactivation in the Conversion of Methanol on Zeolite Catalysts. *J. Catal.* **2009**, *264* (2), 130−137.
(84) Vanoye, L.; Favre-Réguillon, A.; Munno, P.; Rodríguez, J. F.; Dupuy, S.; Pallier, S.; Pitault, I.; De Bellefon, C. Methanol Dehydration over Commercially Available Zeolites: Effect of Hydrophobicity. *Catal. Today* **2013**, *215*, 239−242.
(85) Schnee, J.; Gaigneaux, E. M. Lifetime of the $H_3PW_{12}O_{40}$ Heteropolyacid in the Methanol-to-DME Process: A Question of Pre-Treatment. *Appl. Catal., A* **2017**, *538*, 174−180.
(86) Pérez-Uriarte, P.; Ateka, A.; Gayubo, A. G.; Cordero-Lanzac, T.; Aguayo, A. T.; Bilbao, J. Deactivation Kinetics for the Conversion of Dimethyl Ether to Olefins over a HZSM-5 Zeolite Catalyst. *Chem. Eng. J.* **2017**, *311*, 367−377.
(87) Brunauer, S.; Emmett, P. H.; Teller, E. Adsorption of Gases in Multimolecular Layers. *J. Am. Chem. Soc.* **1938**, *60* (2), 309−319.
(88) Harkins, W. D.; Jura, G. Surfaces of Solids. XIII. A Vapor Adsorption Method for the Determination of the Area of a Solid without the Assumption of a Molecular Area, and the Areas Occupied by Nitrogen and Other Molecules on the Surface of a Solid. *J. Am. Chem. Soc.* **1944**, *66* (8), 1366−1373.
(89) Dubinin, M. M. The Potential Theory of Adsorption of Gases and Vapors for Adsorbents with Energetically Nonuniform Surfaces. *Chem. Rev.* **1960**, *60* (2), 235−241.
(90) Jagiello, J.; Olivier, J. P. 2D-NLDFT Adsorption Models for Carbon Slit-Shaped Pores with Surface Energetical Heterogeneity and Geometrical Corrugation. *Carbon* **2013**, *55*, 70−80.
(91) Thommes, M.; Kaneko, K.; Neimark, A. V.; Olivier, J. P.; Rodriguez-Reinoso, F.; Rouquerol, J.; Sing, K. S. W. IUPAC Technical Report Physisorption of Gases, with Special Reference to

https://doi.org/10.1021/acs.energyfuels.1c01721
Energy Fuels 2021, 35, 17225−17240

the Evaluation of Surface Area and Pore Size Distribution (IUPAC Technical Report). *Pure Appl. Chem.* **2015**, *87* (910), 1051−1069.
(92) Rownaghi, A. A.; Rezaei, F.; Stante, M.; Hedlund, J. Selective Dehydration of Methanol to Dimethyl Ether on ZSM-5 Nanocrystals. *Appl. Catal., B* **2012**, *119*−*120*, 56−61.
(93) Zhao, Z.; Chaos, M.; Kazakov, A.; Dryer, F. L. Thermal Decomposition Reaction and a Comprehensive Kinetic Model of Dimethyl Ether. *Int. J. Chem. Kinet.* **2008**, *40* (1), 1−18.
(94) Martinez-Espin, J. S.; Mortén, M.; Janssens, T. V. W.; Svelle, S.; Beato, P.; Olsbye, U. New Insights into Catalyst Deactivation and Product Distribution of Zeolites in the Methanol-to-Hydrocarbons (MTH) Reaction with Methanol and Dimethyl Ether Feeds. *Catal. Sci. Technol.* **2017**, *7* (13), 2700−2716.
(95) Arfelli, M.; Mattogno, G.; Ferragina, C.; Massucci, M. A. XPS Characterization of γ-Zirconium Phosphate and of Some of Its Intercalation Compounds. A Comparison with the α-Zirconium Phosphate Analogues. *J. Inclusion Phenom. Mol. Recognit. Chem.* **1991**, *11* (1), 15−27.
(96) Liu, R.; Yan, C.; Zhang, C.; Cao, Y.; Long, X. Synthesis of Zirconium Carbide Nanoparticles by Polymerised Complex Route. *Adv. Appl. Ceram.* **2016**, *115* (1), 6−12.
(97) Colón, J. L.; Thakur, D. S.; Yang, C.-Y.; Clearfield, A.; Martini, C. R. X-Ray Photoelectron Spectroscopy and Catalytic Activity of α-Zirconium Phosphate and Zirconium Phosphate Sulfophenylphosphonate. *J. Catal.* **1990**, *124* (1), 148−159.
(98) Xiao, H.; Liu, S. Zirconium Phosphate (ZrP)-Based Functional Materials: Synthesis, Properties and Applications. *Mater. Des.* **2018**, *155*, 19−35.
(99) Alberti, G.; Costantino, U.; Marletta, G.; Puglisi, O.; Pignataro, S. ESCA Investigations of Amorphous and Crystalline Zirconium Acid Phosphates. *J. Inorg. Nucl. Chem.* **1981**, *43* (12), 3329−3334.
(100) Sannigrahi, P.; Ingall, E. Polyphosphates as a Source of Enhanced P Fluxes in Marine Sediments Overlain by Anoxic Waters: Evidence from ^{31}P NMR. *Geochem. Trans.* **2005**, *6* (3), 52−59.
(101) Bortun, A. I.; Butler, C. J. Zirconium Phosphate, Hafnium Phosphate and Method of Makeing Same. WO Patent 2004007360 A1, 2004.
(102) Strelko, V.; Streat, M.; Kozynchenko, O. Preparation, Characterization and Sorptive Properties of Polymer Based Phosphorus-Containing Carbon. *React. Funct. Polym.* **1999**, *41* (1), 245−253.
(103) Díaz, A.; Mosby, B. M.; Bakhmutov, V. I.; Martí, A. A.; Batteas, J. D.; Clearfield, A. Self-Assembled Monolayers Based Upon a Zirconium Phosphate Platform. *Chem. Mater.* **2013**, *25* (5), 723−728.
(104) Bakhmutov, V. I.; Clearfield, A. ^{31}P NMR Relaxation and Motions of Phosphate Groups in Layered Zirconium Phosphate Materials. *J. Phys. Chem. C* **2016**, *120* (34), 19225−19233.
(105) Villa, M.; Chiodelli, G.; Scagliotti, M. P_2O_5 Based Vitreous Electrolytes: Structural Characterization by ^{31}P NMR and Raman Spectroscopies. *Solid State Ionics* **1986**, *18*−*19*, 382−387.
(106) Ruiz-Rosas, R.; Bedia, J.; Rosas, J. M.; Lallave, M.; Loscertales, I. G.; Rodríguez-Mirasol, J.; Cordero, T. Methanol Decomposition on Electrospun Zirconia Nanofibers. *Catal. Today* **2012**, *187* (1), 77−87.
(107) Froment, G. F.; Bischoff, K.; De Wilde, J. *Chemical Reactor Analysis and Design*, 3rd ed.; John Wiley & Sons: Hoboken, NJ, 2011.
(108) Gao, Y.; Chen, S. L.; Wei, Y.; Wang, Y.; Sun, W.; Cao, Y.; Zeng, P. Kinetics of Coke Formation in the Dimethyl Ether-to-Olefins Process over SAPO-34 Catalyst. *Chem. Eng. J.* **2017**, *326*, 528−539.
(109) Zhang, G.; Zhang, X.; Bai, T.; Chen, T.; Fan, W. Coking Kinetics and Influence of Reaction-Regeneration on Acidity, Activity and Deactivation of Zn/HZSM-5 Catalyst during Methanol Aromatization. *J. Energy Chem.* **2015**, *24* (1), 108−118.

https://doi.org/10.1021/acs.energyfuels.1c01721
Energy Fuels 2021, 35, 17225−17240